HHS Public Access

Author manuscript

J Nucl Cardiol. Author manuscript; available in PMC 2015 March 08.

Published in final edited form as:

J Nucl Cardiol. 2009 ; 16(4): 620–639. doi:10.1007/s12350-009-9100-2.

Applications of optical coherence tomography in cardiovascular medicine, Part 2

Joseph W. Villard, MD, MSE[a], **Amit S. Paranjape**[b], **Danielle A. Victor, BS**[c], and **Marc D. Feldman, MD**[a]

[a] Division of Cardiology, University of Texas Health Science Center in San Antonio and the South Texas Veterans Affairs Health System, San Antonio, TX

[b] Department of Biomedical Engineering, University of Texas at Austin, Austin, TX

[c] University of Texas Health Science Center in San Antonio, San Antonio, TX

Drug Eluting Stents and OCT

Introduction

Despite the concerns raised by a well-publicized presentation at the World Congress of Cardiology (WCC) meeting in September 2006,[1] Drug Eluting Stents (DES) have approximately the same short-term and long-term safety profile as Bare Metal Stents (BMS) when used for FDA-labeled indications.[2-5] DES have an in-stent thrombosis rate of 3.6% within 4 years[6] compared to a 3.3% rate for BMS. The main disadvantage of DES is the rate of late complications, specifically stent thrombosis.[4] This usually occurs after the first year and is usually associated with discontinuation of antiplatelet therapy.[7,8] The main benefit of DES is the decreased need for target vessel revascularization,[4] which is enough to be of a clinical advantage in recommending the continued use of DES.[9]

However, there are still some issues that remain to be resolved with DES. The ideal amount of anti-proliferative drug and polymer which strikes the ideal balance between excess neointima formation and restenosis as one extreme, and permanent uncovered struts at the other extreme, has yet to be determined. The duration of antiplatelet therapy needed to minimize late stent thrombosis is still uncertain. Also, the extent to which resistance to aspirin and clopidogrel causes increased thrombosis requires further study. The effects of increased local drug dose due to overlapping stents are still unknown. Finally, the ideal polymer, be it hydrophilic or hydrophobic, which avoids local hypersensitivity reactions in patients have not yet been characterized.

With OCT, clinicians now have an imaging tool that has the resolution and frame rate to study these issues in vivo in patients, rather than only at autopsy. And since OCT presents significantly enhanced resolution compared to IVUS, it is anticipated that OCT will aid in answering these unresolved issues related to DES.

Reprint requests: Marc D. Feldman, MD, Division of Cardiology, University of Texas Health Science Center in San Antonio and the South Texas Veterans Affairs Health System, Mail Code 7872, 7703 Floyd Curl Drive, San Antonio, TX 78229-3900; feldmanm@uthscsa.edu.

Neointima Formation

DES delay neointima formation, thus preventing the most important complication in patients with BMS—restenosis. However, this delay in healing and lack of endothelialization can cause a potentially fatal complication—late-stent thrombosis.[10] The safety of DES could be greatly improved through long-term in vivo studies of neointima formation in patients.

In both animal models and clinical applications of DES, IVUS was shown to be inadequate in the quantification of neointima coverage when compared to histology.[11],[12] OCT, on the other hand, correctly identified the presence and/or absence of tissue coverage for every strut at different time points in a rabbit carotid artery model,[13] using histology as the standard. Since neointima growth cannot be precisely measured by angiography or by IVUS, the use of OCT represents an opportunity to evaluate vascular healing post-stenting.

Recently, strut apposition and thickness of neointimal coverage of sirolimus-eluting stents at 6 months were evaluated by both OCT and IVUS in patients (Figure 1).[14] OCT identified 91% of the struts to be well apposed and covered, 7% well apposed without coverage and 1% mal-apposed and lacking coverage. However, as for the percentage of the neointimal area identified by IVUS, it accounted for only 0-10% in 81% of the SES, because most of the neointima could not be detected by IVUS.[14] In another recent study, a high percentage of struts covered by a thin tissue layer went undetected by IVUS due to its limited resolution[12] but were detected by OCT.

It is anticipated that in vivo patient studies will be performed using OCT to monitor neointimal growth. The number of patients required for studies of novel DES will be dramatically reduced since rather than using an infrequent clinical endpoint such as late stent thrombosis, an alternative endpoint of neointimal coverage could be used as a surrogate. Recently, Finn et al showed the ratio of uncovered to covered struts measured with OCT is an important morphometric predictor of late stent thrombosis. An uncovered strut ratio of greater than 30% was shown to be an indicator of thrombosis at autopsy.[10] As newer generation drug eluting stents focus on the usage of lesser polymer and drug, to allow sufficient intimal hyperplasia to prevent late stent thrombosis, but not enough neointima to result in restenosis, OCT will become more valuable as a tool to examine this trade off.

Brachytherapy

Before the introduction of drug eluting stents, vascular brachytherapy was the first effective anti-proliferative treatment for in-stent restenosis.[15-21] After over a dozen randomized clinical trials,[15-17],[19-26] brachytherapy was shown to be a safe and effective treatment for in stent restenosis. More recent randomized trials have demonstrated that DES are superior to brachytherapy for in stent restenosis in bare metal stents[27] relegating brachytherapy to historical interest at the present time. Although OCT was not available during this era, OCT would have been ideal to investigate the most concerning issue from this time—late stent thrombosis which occurred in approximately 9% of patients undergoing brachytherapy.[28-30] It was hypothesized that brachytherapy prevented neointimal growth, and resulted in nude stent struts. This issue was never totally resolved, and having OCT as a tool could have tested this hypothesis in vivo in patients.

Duration of Anti-platelet Treatment

The duration of anti-platelet therapy is prolonged in patients with DES compared to those with bare metal stents. However, the optimal duration of anti-platelet therapy for patients with DES is unclear at present. The current ACC/AHA/SCAI practice guidelines for the use of anti-platelet agents in patients undergoing elective stent placement recommend that patients should receive clopidogrel 75 mg/day for ≥1 month after implantation of a bare metal stent, ≥3 months after a sirolimus-eluting stent, and ≥6 months after a paclitaxel-eluting stent.[7]

However, it is currently unknown whether longer anti-platelet therapy will reduce the risk for very late stent thrombosis for drug eluting stent. In the ODESSA study,[31] up to 9% of overlapping struts were uncovered a year or more after placement of DES. Can OCT determine at what time all the struts can be expected to develop neointima? What percentage of nude stent struts predicts a low risk of late stent thrombosis, and allow thienopyridines to be discontinued? Which subset of patients will require thienopyridines for life? These issues are currently unresolved and could be addressed by OCT in prospective clinical trials.

Hypersensitivity Reactions to DES

Drug eluting stents consist of metal coated by a polymer with an anti-proliferative drug embedded within the polymer. Though the drug elutes out of the polymer in a matter of weeks, the polymer may never degrade. However, the polymer is known to cause both local and systemic inflammatory reactions,[32],[33] which can also lead to acute stent thrombosis. Current imaging technologies lack the resolution to identify these local inflammatory responses which are composed of eosinophils, T-lymphocytes, and macrophages. Although the current generation of OCT systems cannot image cellular infiltrates in plaque, newer generation systems which are phase sensitive when coupled with OCT contrast agents may have this capability.[34],[35] Thus, OCT has the long-term potential to diagnose these local hypersensitivity reactions in vivo.

“Black Holes” Surrounding Struts

Recent published images of asymptomatic patients with DES, undergoing repeat catheterization and OCT imaging for research, are demonstrating “black holes” surrounding portions of the stent struts, which are of unclear clinical important and composition (Figure 2).

We hypothesize that these areas of signal attenuation (“black holes”) are regions where the arterial wall has retracted from the chronically deployed stent because of localized inflammation due to the polymer. These regions of retraction then fill with both blood and serum. Red cells are known to be broken down and become part of the lipid core.[37],[38] Thus, these are collections of clear fluid and lipid, seen during autopsies of patients with DES, but not bare metal stents (personal communication with Dr. Fermin Tio). Such collections would produce little back scattering of light on OCT imaging and thus appear “black”.

In contrast, these localized areas of signal attenuation are unlikely to be fibrous tissue, cellular infiltrates of inflammatory cells as part of a localized hypersensitivity reaction, or

micro-calcifications. All these structures highly scatter light, and thus would not appear "black".

Overlapping Stents and the Odessa Trial

An overlap of DES raises a concern that double drug and polymer concentrations will be applied to the arterial wall, and may result in localized regions of nude stent struts. For instance, in a balloon-injured rabbit iliac artery,[39] Finn et al placed overlapping DES to study the histopathological response in these areas. At 28 days, there was evidence of delayed endothelialization and increased inflammatory cells in overlapping compared to non-overlapping segments (Figure 3). Because animal models are limited in their ability to replicate clinical conditions, only long-term in vivo human studies using high-resolution OCT imaging will determine whether these findings translate to patients.

The first long-term in vivo patient study to use OCT to examine healing of overlapped DES segments has been completed. The ODESSA trial (Optical coherence tomography in Drug Eluting Stent Safety), performed by Guagliumi and coworkers,[31] evaluated the ratio of uncovered and mal-apposed struts at overlapping versus non-overlapping sites in different DES compared to BMS at 6 months following placement. The study enrolled 77 patients requiring multiple overlapping stents, randomized to receive either sirolimus-eluting stents, paclitaxel eluting-stents, zotarolimus-eluting stents, or bare metal stents.

Results of the trial (Figure 4) show more frequent uncovered struts and mal-apposition in DES compared to BMS, and as high as 9% of nude stent struts at the site of overlap. The clinical implications of this study are unclear at present, but at autopsy, Finn and coworkers[10] showed that patients with acute stent thrombosis had a mean of 30% of nude stent struts, implying that the maximum 9% incidence identified in the ODESSA trial may be clinically benign.

OCT is Superior to IVUS During Stent Examinations

Stent under-expansion, and mal-apposition are critical parameters associated with adverse outcomes[40] with DES. The MATRIX trial[41] demonstrated that liberal use of IVUS before and after DES implantation enhanced the clinical outcomes by ensuring that all the negative parameters mentioned above are minimized. Since OCT has better resolution and faster frame rates, it should improve the clinician's ability to monitor these critical parameters and improve clinical outcomes.

Imaging Vulnerable Plaque with OCT

The most common mechanism for acute coronary syndromes is the rupture of the thin-capped fibroatheroma (TCFA), which is usually less than a 50% diameter stenosis when identified with angiography, with a thin fibrous cap overlying a large lipid core.[42] Specifically, the TCFA is a vulnerable plaque that possesses several key structural features including (1) a thin fibrous cap (<65 μm); (2) a large, necrotizing lipid core; (3) calcium deposits primarily in the form of microcalcifications,[43],[44] and (4) the associated presence of white and/or red thrombus. In order to visualize the arterial wall and determine the vulnerable plaque site, a variety of imaging techniques have been employed including

angiography, angioscopy, computed tomography (CT), magnetic resonance imaging (MRI), intravascular ultrasound (IVUS), and optical coherence tomography (OCT). Since OCT has at least an order of magnitude greater resolution than any of these competing technologies, only OCT has the ability to image thin fibrous caps, micro-calcifications, and identify and differentiate white versus red thrombus, all of which identify a plaque as being vulnerable.

The thin fibrous cap which overlies the necrotic lipid core and is a main predictor of plaque vulnerability.[45] OCT's superior resolution makes it the only imaging modality capable of accurately measuring the thickness of thin fibrous caps, which has been identified to be less than 65 microns at autopsy.[46] Although the penetration depth of OCT is only 2 mm and may not allow the entire plaque to be visualized, this depth is sufficient to accurately define the thin fibrous cap since it is a superficial structure (Figure 5).[47]

Fibrous cap thickness has also been assessed in vivo by OCT. In the first OCT study in order to demonstrate that different plaque morphologies can be visualized in patients with varying clinical presentations, Jang et al[48] showed that the median fibrous cap thickness is significantly different in patients with acute coronary syndrome (47 μm) and stable angina pectoris (102.6 μm). In addition, OCT measurements of fibrous cap thickness have been used to determine the effectiveness of statin therapy. Takarada et al[49] showed that statin treatment increases the thickness of the fibrous cap from 151 ± 110 μm to 280 ± 120 μm in patients with hypercholesterolemia (Figure 6). The lipid core in an OCT image will appear hypodense, signifying a signal poor region, with diffuse borders and an overlying region with high signal corresponding to the fibrous cap.[50],[51] The lipid core is most vulnerable when the lipid pool area is over the threshold (40%) of the plaque cross-sectional area.[43],[44]

As in IVUS, the lipid area within the plaque can be calculated (Figure 7).[50] However, with OCT, the entire lipid core may not be visible due OCT's low penetration depth compared to IVUS. Thus, one of the limitations of OCT is its inability to image the entire lipid core, especially the distal wall, to determine what percent of the plaque cross-sectional area is composed of lipid. Although IVUS may not have the near-field resolution of OCT, IVUS is able to detect lipid pools in the plaque with high sensitivity and specificity (88.9% and 100%, respectively).[52] This fact combined with the high penetration depth of IVUS argues for the development of a combined IVUS/OCT imaging system for quantification of the lipid core size.

Macro-calcifications and calcium nodules in OCT appear as well-delineated regions with sharp borders, but low backscattering within the calcium (Figure 8). In contrast, in IVUS the calcified regions appear as a bright echo signal with acoustic shadowing that can obscure the characteristics of the neighboring tissue[54] so that the borders of heavily calcified regions may be difficult to visualize[55] (Figure 8). Although IVUS has proven to be a viable technique in visualizing large calcifications in the plaque, the same is not true of micro-calcifications where the sensitivity is greatly decreased (64%).[56] OCT has the unique advantage of being the first imaging modality which can image micro-calcifications in vivo.[53],[57] Since the largest light reflection occurs at regions with the greatest index of refraction change, and micro-calcifications with the highest index of refraction of plaque components

are usually nestled within lipid cores with the lowest index of refraction, then micro-calcifications are easily identified by OCT.

The OCT's ability to accurately identify the plaque features including the fibrous cap, lipid core, and calcifications has enabled researchers to classify plaque types according to their structural components. Specifically, Yabushita et al[51] developed criteria to divide plaques into three distinctive types—fibrocalcific (well-delineated signal-poor regions with sharp borders), lipid-rich (signal-poor regions with diffuse borders), and fibrous (homogeneous signal-rich regions) (Figure 9). Postmortem OCT images have shown a sensitivity and specificity ranging from 95% to 96% and 97% for fibrocalcific, 90-94% and 90-92% for lipid-rich, and 71-79% and 97-98% for fibrous plaques when compared with histology.[51] Kume et al[58] also used his classification scheme to differentiate plaques with both OCT and IVUS, achieving similar sensitivities and specificities.

Recently, Kume et al have shown that OCT can be used to differentiate red and white thrombi in postmortem coronary arteries (Figure 10). Red thrombi appear as high back scattering protrusions inside the lumen with a signal free shadow extending abluminally.[59] Since red thrombi are composed mostly of red blood cells, this shadow is expected since red blood cells are known to produce light scattering at wavelengths used for OCT.

White thrombi, on the other hand, appear as signal-rich, low-scattering objects that do not attenuate the OCT signal (Figure 10), allowing the luminal wall to be visualized beyond the thrombus.[59] From this study, Kume et al[59] demonstrated that OCT can differentiate between the red and white thrombi with a sensitivity of 90% and specificity of 88%. These results were confirmed by Meng et al[60] with in vivo rabbit models of thrombosis. White thrombi have recently been identified by our group in vivo on a bare metal stent in a porcine coronary artery, and confirmed by electron microscopy to contain platelets (Figure 11).

Molecular and Cellular Imaging of Atherosclerosis

Since OCT has cellular resolution (<10 microns) in cell culture and simple intact tissues,[61–63] it should be suitable for cellular imaging in intact-diseased human tissues. However, to date cellular imaging has not been successfully performed in patients. We review several attempts at molecular and cellular imaging of the atherosclerotic plaque with OCT and discuss why to date OCT has not been able to achieve this clinical goal.

Cellular Imaging of Macrophages

The presence of macrophages in atherosclerosis is known to predispose to plaque rupture.[42,44,64,65] Notably, OCT has the ability to image other features of the vulnerable plaque (i.e., thin fibrous caps and large lipid cores) and OCT's subcellular resolution (<10 microns; macrophage size = 21.2 ± 0.3 microns[66]) suggest its suitability to image plaque-based macrophages. Consequently, several investigators have attempted imaging of plaque-based macrophages with OCT.[67–71]

Intensity-based Methods Without a Contrast Agent

The first attempt at identifying macrophages in atherosclerotic plaque with OCT was by Tearney et al.[67] Fibrous caps of post-mortem arterial sections were imaged with OCT. Based on known differences of the optical properties of macrophages and surrounding substances such as lipid, these investigators hypothesized that macrophages would produce strong back-reflections and result in a high OCT signal variance. The variance of the OCT signal was determined for the region of interest (ROI) in each sample by post-processing. ROI's with high OCT variance correlated well (r = 0.84) with morphometric measurements of immuno-histochemistry (CD68) in corresponding histology sections (Figure 12). These studies have been extended to patients during heart catheterization for non-ST elevation and ST elevation MI.[67]

The results of this initial study raise questions related to the specificity of this approach. The hypothesis is based on optical property differences within the fibrous cap only, and thus, the technique requires a priori knowledge of the structure of the tissue in which imaging will be performed. In addition, high variance in the OCT signal in these areas may represent back-reflections from other tissue components. For instance, rather than macrophages, micro-calcifications in lipid would offer a larger index of refraction mismatch, and thus provide a larger amount of back reflections of light. Thus, it is possible that the results of Tearney et al are due in part due to micro-calcification of plaque, a known marker for vulnerable plaque. The need for more specific approaches with OCT, possibly in combination with a contrast agent, is clear.[53],[57],[72]

Use of a Cellular Contrast Agent with OCT

To enhance the ability of OCT to perform cellular imaging with greater specificity in intact patient tissues, the use of contrast agents has been proposed.[73],[74] Various approaches have be attempted including chemical enhancers (i.e., absorbing dyes) and contrast agents.[75] First, though nanoparticles are below the resolution of OCT, they could provide a method of contrast enhancement through increased back-scattering of light (ref. Yang). However, little progress has been reported to date using this approach either due to nanoparticle toxicity or to poor in vivo delivery and distribution, both of which imply a difficult transition for use in patients.

To overcome the issues of specific delivery using a non-toxic material, the mannose receptor of the macrophage has been used to target macrophages with dextran-coated nanoparticles by our group and others.[69],[71],[76] Macrophages are then placed in motion and detected by displacement of structures within their microenvironment. Several methods have been used to take advantage of this nanoparticle detection scheme.

Magneto-mechanical Detection of Macrophages

Magnetomotive OCT was recently demonstrated by Oldenburg et al[71] to provide cellular contrast in macrophages which had engulfed iron-oxide nanoparticles. Differential Phase OCT (DP-OCT) was able to visualize magnetically labeled cells in a tissue phantom and in a tadpole by detecting nanometer motion induced by an externally applied magnetic field.

More recently, Oh et al[69,77] reported cellular imaging of atherosclerotic plaque-based macrophages, also with magnetomotive OCT, and distinguished them from other plaque components by identifying macrophages which had engulfed iron-oxide nanoparticles following intravenous injection. These studies were performed ex vivo in a rabbit model of atherosclerosis. Co-localization of nanoparticles with macrophages was confirmed with immuno-histochemistry and Prussian blue stain (Figure 13).[69] However, the difficulty of incorporating an oscillating magnetic field on a catheter tip for clinical applications has led investigators to investigate alternative methods.

Laser-induced thermoelastic expansion for detection of macrophages

Nanoparticles can be fabricated to absorb laser light at different wavelengths.[76,78–80] These synthetic techniques can be advantageous if nanoparticles can be developed which tune to the near infrared, since at these wavelengths there is a window where competition for light absorption by tissue components are at a minimum.[81,82] After being engulfed by macrophages, nanoparticles absorb pulsed laser light and convert that energy into localized temperature oscillations.[70] These temperature oscillations result in thermoelastic expansion of the surrounding microenvironment which can be detected by OCT.

Recently, Kim et al[70] used this detection scheme in a rabbit model of atherosclerosis injected with monocrystalline iron-oxide nanoparticles (MIONs). Postmortem atherosclerotic tissue was excited by a 532-nm pulsed laser light and the thermoelastic displacement at the surface of the tissue was detected by Differential Phase-OCT. This study showed for the first time that Differential Phase-OCT could detect laser-induced thermoelastic expansion in plaque-based macrophages tagged with nanoparticles.

Adler et al[68] demonstrated detection of these temperature oscillations for the first time with Phase-Sensitive OCT rather than Differential Phase-OCT. The investigators imaged phantoms with gold nanoshells excited by a 808-nm pulsed-laser light and observed a high contrast between solutions containing nanoshells and solutions without nanoshells. In comparison to DP-OCT, phase-sensitive OCT can be used with Fourier-domain OCT systems thus allowing for much faster imaging and can be incorporated into an intravascular catheter allowing for in vivo imaging. Another advantage of Adler's technique is incorporation of gold nanoshells that absorb 808-nm light in the clinically important diagnostic and therapeutic near-infrared window (see Part 1 of this review).

Subsequently, researchers at the University of Texas fabricated a novel nanoparticle.[76] capable of both tagging the plaque-based macrophages and absorbing light in the near-infrared window. After injecting these gold/iron-oxide nanoparticles into a double-balloon injured rabbit model of atherosclerosis, laser-induced thermal detection of macrophages was possible with phase-sensitive OCT. Thus, for the first time, plaque-based macrophages were distinguished from competing plaque components by OCT in the clinically important near-infrared window.[76,83]

Molecular Imaging of Plaque Components

Spectroscopy can analyze biochemical composition of tissue and detect molecular markers of disease, but spectroscopic techniques do not provide structural or morphological

information of the lesion. With a combination of OCT and spectroscopic techniques, both tissue microstructure and biochemical composition could be determined and a fusion image which overlays both could be generated.

Raman Spectroscopy and OCT

Raman Spectroscopy (RS) uses the inelastic scattering of light to analyze vibrational and rotational modes of molecules. Laser light is directed onto a tissue via an optical fiber and back-reflected light is collected and analyzed in a spectrometer. The resulting molecular fingerprint allows a biochemical analysis of the constituents of tissue.[84]

The molecular characteristics of calcium, cholesterol, and collagen allow for a highly specific biochemical analysis of diseased coronary arteries (Figure 14).[85] Using RS, Silveira et al analyzed the components of 111 arteries and developed an algorithm that correctly classified 95 of those coronary artery fragments as non-atherosclerotic, atherosclerotic without calcification, and atherosclerotic with calcification. Later, the same group used Fourier-Transform RS to correctly classify 71 out of 75 post-mortem carotid arteries.[86] Similarly, Buschman et al[87] combined the independent spectra of the various components of atherosclerotic plaque to arrive at a diagnostic algorithm that correctly classified 64 out of 68 coronary artery samples.

In 2000, Romer et al reported a successful combination of IVUS and RS in an *ex vivo* study of coronary arteries. With this setup, they were able to accurately locate and quantify calcium salts and cholesterol within arteries.[88] This experiment demonstrated the complementary nature of the two modalities: real-time guidance of RS acquisition by IVUS and obtaining a biochemical fingerprint of structures seen with IVUS.

More recently, Patil et al[84] demonstrated the use of a dual-modal device capable of acquiring OCT and RS data through a common optical fiber. Thus, as with RS-IVUS, real time imaging with OCT can be used to guide RS acquisition, but at a much higher resolution. RS-OCT successfully identified collagen in a healing scab and malignant cells in breast cancer[84]; however, cardiovascular applications have yet to be reported. Further development of this technique for intravascular applications would require a catheter-based system and would require blood clearance during imaging. Some of the shortcomings of RS are reduced penetration depth compared with OCT (hundreds of microns versus 1-2 mm) and the low signal-to-noise ratio of RS.[86]

NIR Spectroscopy and OCT

The NIR reflectance spectroscopy uses infrared light between 800 and 2500 nm.[89] Light enters arterial tissue, is scattered, absorbed, and back-reflected into the optical probe. The result is an absorbance spectrum unique to the biochemical composition of the tissue (Figure 15) similar to the biochemical fingerprint of RS. An advantage of NIR spectroscopy over RS is its increased penetration depth (2 mm versus 0.3 mm) similar to that of OCT[89]; however, a disadvantage is that of its reduced specificity when compared to RS.[89]

NIR spectroscopy helps to discriminate vulnerable from stable plaque due to the unique spectra obtained from TCFAs, lipid-rich and inflammatory plaques.[90] Moreno et al found a

sensitivity of 90% and a specificity of 93% in the detection of lipid-rich plaques using NIR spectroscopy. The sensitivity and specificity for other features of vulnerable plaque ranged from 77% to 93%.[90] Several other studies have reported similar accuracy in identifying vulnerable plaque with NIR spectroscopy.[89]

Recently, a catheter-based NIR spectroscopy system has been cleared by the FDA for use in patients to identify lipid-rich plaques.[91] The LipiScan™ Coronary Imaging System from InfraReDex, Inc. (Burlington, MA) contains an optical probe that spins as it collects NIR spectra from the wall of the vessel, mechanically similar to an intravascular OCT system (see Part 1 of this review). The LipiScan™ system creates a three-dimensional biochemical map (a Chemogram™) of the vessel wall that identifies the presence or absence of lipid-rich plaques. Initial clinical studies with the device demonstrate its ability to detect lipid-rich plaques in patients.[91] Notably, the system is able to perform without clearing the vessel of red blood cells during imaging[91]; however, it would likely benefit from the flushing that must be performed during OCT imaging, since more light would return to the optical probe during blood clearance.

The LipiScan™ system has not yet been combined with an OCT system, but obvious advantages exist from this combination. A single, intravascular, catheter-based optical probe with the structural imaging capabilities of OCT in combination with the molecular imaging capabilities of NIR spectroscopy could combine multiple indicators of vulnerability (particularly fibrous cap thickness and the presence of a lipid core) to improve the sensitivity and specificity of vulnerable plaque detection.

Future Technologies

An intravascular Optical Coherence Tomography (OCT) imaging system can be subdivided into three major components. These three components are (1) Catheter, (2) Optical Instrumentation, and (3) Computer acquisition and software. Future technologies will focus on improving all the three components of the intravascular OCT system.

Catheters in Intravascular OCT systems

Currently, intravascular OCT systems spin the catheter with the motor located outside the catheter itself. Such catheters are broadly called mechanically actuated catheters. Mechanical catheters show a distinct variation in rotational speed causing an artifact called non-uniform rotational distortion (NURD), similar to that seen with IVUS. NURD is caused by the mechanical friction within the catheter rotating mechanism. NURD is visible as a circumferential stretching of a portion of the image with the contralateral arterial wall exhibiting circumferential compression. Kawase et al[92] have studied the effect of NURD on IVUS images.

Spinning Tip Catheters

It is expected that a new family of catheters will gradually supersede these mechanically actuated catheters. The focus of recent developments in catheter technology is on miniaturizing the actuating mechanism and placing it in the tip of the catheter.[93] This family of catheters is broadly called “spinning tip catheters.” Spinning-tip catheters enable high-

speed imaging, since they provide higher rates of angular rotational velocity without being affected by NURD. In 2004, Herz et al[93] demonstrated a distally actuated, rotational-scanning micromotor endoscope catheter probe. Using this probe, in vivo endoscopic OCT imaging of a rabbit colon was demonstrated, with significantly less NURD.

As micro-electro-mechanical systems (MEMS) technology rapidly advances, we expect MEMS-based devices to play an important role in spinning tip catheter fabrication. MEMS is the integration of mechanical elements, sensors, actuators, and electronics on a common silicon chip using microfabrication technology.[94] This ability of MEMS enables us to integrate an entire system on one small chip, thus providing an efficient mechanism for miniaturizing OCT scanning systems. MEMS scanners also provide reliable high-speed scanning at low power consumption, making them suitable for integration into in vivo imaging devices. Bouma et al[95] demonstrated a spectral domain OCT system with a catheter incorporating a MEMS micro-mirror scanner. They were able to demonstrate fast scanning rates of up to 18,500 Ascans/sec and were able to acquire both intensity and polarization images.

Imaging speeds could be increased if catheters had multiple optical fibers on a single catheter. In such a method, spinning would not be necessary. This faster imaging could be achieved using multifiber-phased array geometry analogous to that used in 2D transthoracic echocardiography. Yeh et al[96] have demonstrated the use of such a fiber in IVUS systems but practical implementation of such a catheter in human IV-OCT systems has not yet been achieved.[36]

Transition to Spectral Domain Systems

The OCT instrumentation has seen some rapid advances since the early part of this decade. One of the major hurdles with using OCT for cardiovascular imaging has been the problem of the red blood cells scattering the imaging light.[97-100] Several solutions have been reviewed in Part 1 to eliminate this problem of light attenuation. Since reduced imaging times result in reduced flush, efforts in OCT instrumentation will concentrate on increasing the acquisition speed of OCT devices. Spectral domain techniques (also called as Optical Frequency Domain Imaging and Fourier Domain Imaging (OFDI) Techniques) are the most significant development toward reducing imaging times.

Time-domain techniques are somewhat limited in their efficient light utilization and require slower pull-backs of about 1 mm/second to allow adequate collection of reflected light. The cause of the slower imaging speed is the need to mechanically scan the reference arm. Spectral domain techniques dramatically improve imaging speed by eliminating the need for mechanical scanning of the reference arm. Spectral domain techniques also offer the added advantage of reduced light losses during a single scan improving the signal-to-noise ratio in the process.[101] Thus, the biggest advantage of moving to the spectral (OFDI) domain technique is its better imaging quality at higher speed than time-domain OCT techniques.

The first implementation of OFDI was by researchers at the Harvard Wellman Center for Photomedicine. They demonstrated that wavelength-swept narrowband laser sources which provide improved imaging quality, imaging depth, and speed can be used for a spectral

domain OCT system. First, Yun et al[102] demonstrated a swept-source laser which could be used in an OCT system. Later, in 2004, they demonstrated a Fourier-domain OCT implementation based on this swept-source laser. However, the drawback of this OCT system was that it was heavily dependent on the quality and stability of the source.[103,104] One major limitation for swept-source lasers is the speed at which the laser sweeps. Future developments will concentrate on optimizing the laser quality, and this holds the potential for dramatically improving swept-source OCT.

We expect that swept-source-laser speed limitations will be overcome using Fourier-Domain Mode Locked (FDML) lasers. The first demonstration of this advanced laser was by Fujimoto et al.[105] Figure 16 shows various examples of OCT images obtained using an FDML laser. FDML lasers exhibit dramatically improved coherence and noise properties, compared with other rapidly swept lasers. Furthermore, they have no fundamental limitation in sweep rate, which means they can be used to achieve high quality OCT imaging at record speeds of up to 370,000 lines per second.[106]

Polarization Sensitive OCT

Polarization sensitive OCT (PS-OCT) is expected to add a new dimension for the use of OCT to characterize tissue.[107] A stable fibrous cap is predominantly composed of collagen synthesized by intimal smooth muscle cells (SMCs). The mechanisms leading to plaque instability include the proteolysis of collagen by metalloproteinases released by activated macrophages and apoptosis of intimal SMCs. The net effect of these mechanisms is the transition from a stable to a vulnerable fibrous cap.[108-110] PS-OCT gives us a measure of the collagen content of tissues. PS-OCT has been successfully applied by Nadkarni et al[107] to measure collagen and SMC content in plaque. PS-OCT analyzes the polarization state of the light reflected from tissue being imaged. Figure 17, adapted from Nadkarni et al[107,111] shows an OCT image and corresponding PS-OCT image of fibrous plaque. This figure illustrates how PS-OCT is able to provide additional information regarding fibrous tissue content of the fibrous cap, and cap stability.

We expect that next generation PS-OCT systems will use two incident beams as demonstrated by Oh et al.[112] Intravascular catheter systems are subjected to a wide variety of pressure and motion changes, caused principally by the blood flow, the tortuosity of the vessels, and the motion of the heart. These changes in pressure and motion cause the polarization measurements recorded to become inaccurate. A two-beam system is able to calibrate out these sources of error caused by the motion and pressure changes in the vessels. With these more advanced systems in use, researchers were able to image a human coronary artery ex vivo through a flexible fiber-optic catheter with high speed. The application of PS-OCT in vivo has not yet been achieved to date.

Speckle Reduction

Speckle is a type of “noise” that degrades OCT images. When laser light strikes the surface being imaged, the light is reflected back.[113] The surface roughness has microscopic variations. These variations cause the reflected light to be brighter in some spots and darker at others. This intensity variation of reflected light is called speckle. Speckle is what has

prevented OCT from achieving cellular resolution in complex in vivo tissues, which would be typical of a clinical environment. Speckle reduction techniques will in the future provide much higher-quality OCT images. Two strategies can be utilized for reducing speckle in OCT. The first approach involves modifying the OCT instrumentation to reduce the effect of speckle. The second one involves using software modifications for speckle reduction.

In 2003, Iftima et al[114] used the hardware modification approach to reduce speckle. They proposed a new method of averaging multiple images acquired at multiple incident angles. This approach can be used with existing probe technology and is capable of increasing signal-to-noise ratio (SNR) and reduced speckle. This method holds the promise of being a cost effective method requiring minimal system modifications. Pircher et al[115] used two incident beams of light to acquire two different images at different wavelengths. The final image, which was an average of the images acquired at the two different wavelengths showed an improved SNR and reduced speckle. This method, however, has the drawback of requiring two sources at different wavelengths.

In the future, we anticipate software-based methods of speckle reduction will significantly impact intravascular OCT systems. Software methods have the inherent advantage of being cost effective. However, since software-based methods often involve post-processing, they cannot be used in real time. Rapid hardware changes will make real time implementation of software-based methods a reality in the not-too-distant future. A software-based approach has been demonstrated by Ozcan et al.[116] Adler et al[117] used a wavelet-based filtering approach to reduce the effect of speckle.

Laser Speckle Imaging (LSI) and Speckle Analysis

Approaches using speckle analysis are an important advancement when characterizing the fibrous cap. Speckle analysis provides an innovative tool in characterizing fibrous cap thickness because thin and thick cap fibroatheromas have different biomechanical properties that laser speckle imaging (LSI) can identify. In 2001, Tearney and Bouma[118] demonstrated a technique for plaque characterization using speckle analysis. They used speckle-pattern fluctuations arising out of the differences in the biomechanical properties of fibroatheroma for characterizing plaque. These studies were, however, conducted ex-vivo.

Translation of LSI into in vivo systems involves overcoming several hurdles. Laser speckle pattern has to be transmitted from the coronary wall to the image detector in the presence of cardiac motion using small-diameter, flexible optical fiber bundles. However, these multifiber bundles suffer from inter-fiber leakage of light. In 2008, Nadkarni et al[111] successfully solved this problem using a newly designed fiber optic bundle. The use of speckle analysis techniques offers a new way to distinguish between stable and unstable plaque.

Combined IVUS and OCT Devices

Future trends in intravascular OCT will include a combination or fusion of IVUS and OCT technologies into a common catheter. Both IVUS and OCT complement each other for detection and characterization of vulnerable plaque compared to using a single technology in stand-alone mode. OCT can determine the thickness off the fibrous cap, while IVUS cannot.

OCT can be used to visualize macrophages while IVUS cannot. Speckle OCT can be used for determining plaque vulnerability. However, OCT cannot visualize the entire lipid pool size because of limited penetration depth, but IVUS with its ability to penetrate deeper and visualize the back wall of the lipid pool. The IVUS is also capable of determining “plaque burden,” lacking in OCT due to its limited depth of penetration.

A combination of OCT and IVUS also holds the promise of being a better tool for stent deployment. IVUS has the ability to detect medial and adventitial borders for sizing the diameter of stents. The OCT with its intrinsic advantages of better identification of whether a stent is fully expanded due to its ability to image the stent-lumen wall contact, can be used to avoid mal-apposition. Huang et al[119] have even demonstrated the use of ultrasound to enhance the penetration depth of OCT. Thus, combining IVUS with OCT not only has a complementary benefit but may actually improve the OCT image. Thus, combining the inherent advantages of OCT and IVUS gives cardiologists an improved tool for diagnosing and even treating fibroatheroma.

Conclusion

In conclusion, OCT will play a pivotal in the next several years teaching us which DES designs will be ideal as less polymer and drug usage is adopted. Further, the clinical relevance of nude stent struts, duration of anti-platelet drugs, and new finding of “black holes” surrounding stent struts will be determined, because of OCT's greater resolution over other imaging modalities available in the catheterization laboratory. In the future, a combination of OCT and spectroscopic techniques would provide several advantages in vulnerable plaque detection. First, OCT would provide real-time guidance of biochemical analysis. In addition, co-localization of tissue microstructure with chemical composition would be realized. Finally, a combination of vulnerability features detectable by OCT (e.g., TCFA and macrophages) and spectroscopy (lipid cores, macrophages, calcium, etc.) could provide an extremely accurate test for vulnerability.

Acknowledgments

The authors, JWV and ASP, have received funding from NIH under Grant # HL07446 and 5R01EY016462, respectively, DAV has received financial support as ‘The Palmaz Gift to the MD/PhD program at UTHSCSA’, and MFD from the VA Merit.

References

1. Camendzind, E.; Nordman, AJ.; Briel, M.; Bucher, HC. Safety of drug eluting stents: Insights from a meta-analysis. Presented at the European Society of Cardiology Annual Congress; 2006. Hotline I
2. Stone GW, Moses JW, Ellis SG, Schofer J, Dawkins KD, Morice MC, et al. Safety and efficacy of sirolimus- and paclitaxel-eluting coronary stents. N Engl J Med. 2007; 356:998–1008. [PubMed: 17296824]
3. Stettler C, Wandel S, Allemann S, Kastrati A, Morice MC, Schomig A, et al. Outcomes associated with drug-eluting and bare-metal stents: A collaborative network meta-analysis. Lancet. 2007; 370:937–48. [PubMed: 17869634]
4. Rizik DG, Klassen KJ. Assessing the landscape of stent thrombosis: The drug-eluting versus bare-metal stent controversy. Am J Cardiol. 2008; 102:4J–11J.

5. Spaulding C. The question of drug-eluting stent safety: Then and now. Am J Cardiol. 2008; 102:12J–7J. [PubMed: 18572029]

6. Mauri L, Hsieh WH, Massaro JM, Ho KK, D'Agostino R, Cutlip DE. Stent thrombosis in randomized clinical trials of drug-eluting stents. N Engl J Med. 2007; 356:1020–9. [PubMed: 17296821]

7. King SB III, Smith SC Jr, Hirshfeld JW Jr, Jacobs AK, Morrison DA, Williams DO, et al. 2007 Focused update of the ACC/AHA/SCAI 2005 guideline update for percutaneous coronary intervention: A report of the American College of Cardiology/American Heart Association Task Force on Practice Guidelines: 2007 Writing Group to Review New Evidence and Update the ACC/AHA/SCAI 2005 Guideline Update for Percutaneous Coronary Intervention, Writing on Behalf of the 2005 Writing Committee. Circulation. 2008; 117:261–95. [PubMed: 18079354]

8. Ellis SG, Colombo A, Grube E, Popma J, Koglin J, Dawkins KD, et al. Incidence, timing, and correlates of stent thrombosis with the polymeric paclitaxel drug-eluting stent: A TAXUS II, IV, V, and VI meta-analysis of 3, 445 patients followed for up to 3 years. J Am Coll Cardiol. 2007; 49:1043–51. [PubMed: 17349883]

9. US Food and Drug Administration. Update to FDA statement on coronary drug-eluting stents. 20 April 2009Available at: http://www.fda.gov/cdrh/news/010407.html

10. Finn AV, Joner M, Nakazawa G, Kolodgie F, Newell J, John MC, et al. Pathological correlates of late drug-eluting stent thrombosis: Strut coverage as a marker of endothelialization. Circulation. 2007; 115:2435–41. [PubMed: 17438147]

11. Chen BX, Ma FY, Luo W, Ruan JH, Xie WL, Zhao XZ, et al. Neointimal coverage of bare-metal and sirolimus-eluting stents evaluated with optical coherence tomography. Heart. 2008; 94:566–70. [PubMed: 17923466]

12. Takano M, Inami S, Jang IK, Yamamoto M, Murakami D, Seimiya K, et al. Evaluation by optical coherence tomography of neointimal coverage of sirolimus-eluting stent three months after implantation. Am J Cardiol. 2007; 99:1033–8. [PubMed: 17437723]

13. Prati F, Cera M, Ramazzotti V, Imola F, Giudice R, Giudice M, et al. From bench to bedside: A novel technique of acquiring OCT images. Circ J. 2008; 72:839–43. [PubMed: 18441468]

14. Matsumoto D, Shite J, Shinke T, Otake H, Tanino Y, Ogasawara D, et al. Neointimal coverage of sirolimus-eluting stents at 6-month follow-up: Evaluated by optical coherence tomography. Eur Heart J. 2007; 28:961–7. [PubMed: 17135281]

15. Teirstein PS, Massullo V, Jani S, Popma JJ, Mintz GS, Russo RJ, et al. Catheter-based radiotherapy to inhibit restenosis after coronary stenting. N Engl J Med. 1997; 336:1697–703. [PubMed: 9180087]

16. Waksman R, White RL, Chan RC, Bass BG, Geirlach L, Mintz GS, et al. Intracoronary gamma-radiation therapy after angioplasty inhibits recurrence in patients with in-stent restenosis. Circulation. 2000; 101:2165–71. [PubMed: 10801757]

17. Leon MB, Teirstein PS, Moses JW, Tripuraneni P, Lansky AJ, Jani S, et al. Localized intracoronary gamma-radiation therapy to inhibit the recurrence of restenosis after stenting. N Engl J Med. 2001; 344:250–6. [PubMed: 11172151]

18. Ajani AE, Waksman R. Intracoronary beta radiation: State of the art. J Interv Cardiol. 2001; 14:601–9. [PubMed: 12053381]

19. Waksman R, Raizner AE, Yeung AC, Lansky AJ, Vandertie L. Use of localised intracoronary beta radiation in treatment of instent restenosis: The INHIBIT randomised controlled trial. Lancet. 2002; 359:551–7. [PubMed: 11867107]

20. Waksman R, Ajani AE, White RL, Chan RC, Satler LF, Kent KM, et al. Intravascular gamma radiation for in-stent restenosis in saphenous-vein bypass grafts. N Engl J Med. 2002; 346:1194–9. [PubMed: 11961147]

21. Popma JJ, Suntharalingam M, Lansky AJ, Heuser RR, Speiser B, Teirstein PS, et al. Stents And Radiation Therapy (START) Investigators. Randomized trial of 90Sr/90Y beta-radiation versus placebo control for treatment of in-stent restenosis. Circulation. 2002; 106:1090–6. [PubMed: 12196334]

22. King SB 3rd, Williams DO, Chougule P, Klein JL, Waksman R, Hilstead R, et al. Endovascular beta-radiation to reduce restenosis after coronary balloon angioplasty: Results of the beta energy restenosis trial (BERT). Circulation. 1998; 97:2025–30. [PubMed: 9610532]
23. Raizner AE, Oesterle SN, Waksman R, Serruys PW, Colombo A, Lim YL, et al. Inhibition of restenosis with beta-emitting radio-therapy: Report of the Proliferation Reduction with Vascular Energy Trial (PREVENT). Circulation. 2000; 102:951–8. [PubMed: 10961957]
24. Verin V, Popowski Y, de Bruyne B, Baumgart D, Sauerwein W, Lins M, et al. Endoluminal beta-radiation therapy for the prevention of coronary restenosis after balloon angioplasty. The Dose-Finding Study Group. N Engl J Med. 2001; 344:243–9. [PubMed: 11172150]
25. Sapirstein W, Zuckerman B, Dillard J. FDA approval of coronary-artery brachytherapy. N Engl J Med. 2001; 344:297–9. [PubMed: 11172159]
26. Grise MA, Massullo V, Jani S, Popma JJ, Russo RJ, Schatz RA, et al. Five-year clinical follow-up after intracoronary radiation: Results of a randomized clinical trial. Circulation. 2002; 105:2737–40. [PubMed: 12057987]
27. Stone GW, Ellis SG, O'Shaughnessy CD, Martin SL, Satler L, McGarry T, et al. Paclitaxel-eluting stents vs vascular brachytherapy for in-stent restenosis within bare-metal stents: The TAXUS V ISR randomized trial. JAMA. 2006; 295:1253–63. [PubMed: 16531618]
28. Costa MA, Sabate M, van der Giessen WJ, Kay IP, Cervinka P, Ligthart JMR, et al. Late coronary occlusion after intracoronary brachytherapy. Circulation. 1999; 100:789–92. [PubMed: 10458712]
29. Waksman R. Late thrombosis after radiation: Sitting on a time bomb. Circulation. 1999; 100:780–2. [PubMed: 10458709]
30. N Novoste Corporation Ga. Clinical trials. 25 April 2009Available at: http://www.bestvascular.com/healthcare/hcp_trials.html
31. Guagliumi G. ODESSA: A prospective randomized study using OCT to evaluate strut coverage of Sirolimus-eluting, Paclitaxel-eluting, and Zotarolimus-eluting coronary stents. TCT. 2008; 68
32. Virmani R, Guagliumi G, Farb A, Musumeci G, Grieco N, Motta T, et al. Localized hypersensitivity and late coronary thrombosis secondary to a sirolimus-eluting stent: Should we be cautious? Circulation. 2004; 109:701–5. [PubMed: 14744976]
33. Nebeker JR, Virmani R, Bennett CL, Hoffman JM, Samore MH, Alvarez J, et al. Hypersensitivity cases associated with drug-eluting coronary stents: A review of available cases from the Research on Adverse Drug Events and Reports (RADAR) project. J Am Coll Cardiol. 2006; 47:175–81. [PubMed: 16386683]
34. Oldenburg AL, Crecea V, Rinne SA, Boppart SA. Phase-resolved magnetomotive OCT for imaging nanomolar concentrations of magnetic nanoparticles in tissues. Opt Express. 2008; 16:11525–39. [PubMed: 18648474]
35. Aaron JS, Oh J, Larson TA, Kumar S, Milner TE, Sokolov KV. Increased optical contrast in imaging of epidermal growth factor receptor using magnetically actuated hybrid gold/iron oxide nanoparticles. Opt Express. 2006; 14:12930–43. [PubMed: 19532186]
36. Guagliumi G, Sirbu V. Optical coherence tomography: High resolution intravascular imaging to evaluate vascular healing after coronary stenting. Catheter Cardiovasc Interv. 2008; 72:237–47. [PubMed: 18655155]
37. Virmani R, Kolodgie FD, Burke AP, Finn AV, Gold HK, Tulenko TN, et al. Atherosclerotic plaque progression and vulnerability to rupture: Angiogenesis as a source of intraplaque hemorrhage. Arterioscler Thromb Vasc Biol. 2005; 25:2054–61. [PubMed: 16037567]
38. Kolodgie FD, Gold HK, Burke AP, Fowler DR, Kruth HS, Weber DK, et al. Intraplaque hemorrhage and progression of coronary atheroma. N Engl J Med. 2003; 349:2316–25. [PubMed: 14668457]
39. Finn AV, Kolodgie FD, Harnek J, Guerrero LJ, Acampado E, Tefera K, et al. Differential response of delayed healing and persistent inflammation at sites of overlapping sirolimus- or paclitaxel-eluting stents. Circulation. 2005; 112:270–8. [PubMed: 15998681]
40. Moses JW, Dangas G, Mehran R, Mintz GS. Drug-eluting stents in the real world: How intravascular ultrasound can improve clinical outcome. Am J Cardiol (suppl). 2008; 102:24J–8J.
41. Dangas GD, Mehran R, Moses JW. Long-term safety of drug eluting stents in off-label use: Results of the MATRIX registry. ACC 2007. Late Breaking Trial Session.

42. Kolodgie FD, Virmani R, Burke AP, Farb A, Weber DK, Kutys R, et al. Pathologic assessment of the vulnerable human coronary plaque. Heart. 2004; 90:1385–91. [PubMed: 15547008]
43. Libby P. Coronary artery injury and the biology of atherosclerosis: Inflammation, thrombosis, and stabilization. Am J Cardiol. 2000; 86:3J–8J. discussion 8J-9J.
44. Davies MJ, Richardson PD, Woolf N, Katz DR, Mann J. Risk of thrombosis in human atherosclerotic plaques: Role of extracellular lipid, macrophage, and smooth muscle cell content. Br Heart J. 1993; 69:377–81. [PubMed: 8518056]
45. Burke AP, Farb A, Malcom GT, Liang YH, Smialek J, Virmani R. Coronary risk factors and plaque morphology in men with coronary disease who died suddenly. N Engl J Med. 1997; 336:1276–82. [PubMed: 9113930]
46. Brezinski ME, Tearney GJ, Weissman NJ, Boppart SA, Bouma BE, Hee MR, et al. Assessing atherosclerotic plaque morphology: Comparison of optical coherence tomography and high frequency intravascular ultrasound. Heart. 1997; 77:397–403. [PubMed: 9196405]
47. Kume T, Akasaka T, Kawamoto T, Okura H, Watanabe N, Toyota E, et al. Measurement of the thickness of the fibrous cap by optical coherence tomography. Am Heart J. 2006; 152:755.e1–4. [PubMed: 16996853]
48. Jang IK, Tearney GJ, MacNeill B, Takano M, Moselewski F, Iftima N, et al. In vivo characterization of coronary atherosclerotic plaque by use of optical coherence tomography. Circulation. 2005; 111:1551–5. [PubMed: 15781733]
49. Takarada S, Imanishi T, Kubo T, Tanimoto T, Kitabata H, Nakamura N, et al. Effect of statin therapy on coronary fibrous-cap thickness in patients with acute coronary syndrome: Assessment by optical coherence tomography study. Atherosclerosis. 2009; 202:491–7. [PubMed: 18572175]
50. Cilingiroglu M, Oh JH, Sugunan B, Kemp NJ, Kim J, Lee S. Detection of vulnerable plaque in a murine model of atherosclerosis with optical coherence tomography. Catheter Cardiovasc Interv: Official J Soc Cardiac Angiogr. 2006; 67(6):915–23.
51. Yabushita H, Bouma BE, Houser SL, Aretz HT, Jang IK, Schlendorf KH, et al. Characterization of human atherosclerosis by optical coherence tomography. Circulation. 2002; 106:1640–5. [PubMed: 12270856]
52. Di Mario C, The SH, Madretsma S, van Suylen RJ, Wilson RA, Bom N, et al. Detection and characterization of vascular lesions by intravascular ultrasound: An in vitro study correlated with histology. J Am Soc Echocardiogr. 1992; 5:135–46. [PubMed: 1571167]
53. Cilingiroglu M, Oh JH, Sugunan B, Kemp NJ, Kim J, Lee S, et al. Detection of vulnerable plaque in a murine model of atherosclerosis with optical coherence tomography. Catheter Cardiovasc Interv. 2006; 67:915–23. [PubMed: 16602128]
54. Jang IK, Bouma BE, Kang DH, Park SJ, Park SW, Seung KB, et al. Visualization of coronary atherosclerotic plaques in patients using optical coherence tomography: Comparison with intravascular ultrasound. J Am Coll Cardiol. 2002; 39:604–9. [PubMed: 11849858]
55. Ferencik M, Chan RC, Achenbach S, Lisauskas JB, Houser SL, Hoffmann U, et al. Arterial wall imaging: Evaluation with 16-section multidetector CT in blood vessel phantoms and ex vivo coronary arteries. Radiology. 2006; 240:708–16. [PubMed: 16857982]
56. Friedrich GJ, Moes NY, Muhlberger VA, Gabl C, Mikuz G, Hausmann D, et al. Detection of intralesional calcium by intracoronary ultrasound depends on the histologic pattern. Am Heart J. 1994; 128:435–41. [PubMed: 8074002]
57. Mancuso JJ, Cheruku K, Kemp NJ, Milner TE, Banas C, Tio FO, et al. Peripheral artery composition evaluated with OCT. Endovasc Today. 2008; 7:26–30.
58. Kume T, Akasaka T, Kawamoto T, Watanabe N, Toyota E, Neishi Y, et al. Assessment of coronary arterial plaque by optical coherence tomography. Am J Cardiol. 2006; 97:1172–5. [PubMed: 16616021]
59. Kume T, Akasaka T, Kawamoto T, Ogasawara Y, Watanabe N, Toyota E, et al. Assessment of coronary arterial thrombus by optical coherence tomography. Am J Cardiol. 2006; 97:1713–7. [PubMed: 16765119]
60. Meng L, Lv B, Zhang S, Yv B. In vivo optical coherence tomography of experimental thrombosis in a rabbit carotid model. Heart. 2008; 94:777–80. [PubMed: 17947363]

61. Huang D, Swanson EA, Lin CP, Schuman JS, Stinson WG, Chang W. Optical coherence tomography. Science (New York, NY). 1991; 254:1178–81.
62. Brezinski ME, Tearney GJ, Bouma BE, Izatt JA, Hee MR, Swanson EA, et al. Optical coherence tomography for optical biopsy. Properties and demonstration of vascular pathology. Circulation. 1996; 93:1206–13. [PubMed: 8653843]
63. Fujimoto JG, Boppart SA, Tearney GJ, Bouma BE, Pitris C, Brezinski ME. High resolution in vivo intra-arterial imaging with optical coherence tomography. Heart. 1999; 82:128–33. [PubMed: 10409522]
64. Davies MJ, Thomas AC. Plaque fissuring—the cause of acute myocardial infarction, sudden ischaemic death, and crescendo angina. Br Heart J. 1985; 53:363–73. [PubMed: 3885978]
65. Virmani R, Kolodgie FD, Burke AP, Farb A, Schwartz SM. Lessons from sudden coronary death: A comprehensive morphological classification scheme for atherosclerotic lesions. Arterioscler Thromb Vasc Biol. 2000; 20:1262–75. [PubMed: 10807742]
66. Krombach F, Munzing S, Allmeling AM, Gerlach JT, Behr J, Dorger M. Cell size of alveolar macrophages: An interspecies comparison. Environ Health Perspect. 1997; 105(Suppl 5):1261–3. [PubMed: 9400735]
67. Tearney GJ, Yabushita H, Houser SL, Aretz HT, Jang IK, Schlendorf KH, et al. Quantification of macrophage content in atherosclerotic plaques by optical coherence tomography. Circulation. 2003; 107:113–9. [PubMed: 12515752]
68. Adler DC, Huang SW, Huber R, Fujimoto JG. Photothermal detection of gold nanoparticles using phase-sensitive optical coherence tomography. Opt Express. 2008; 16:4376–93. [PubMed: 18542535]
69. Oh J, Feldman MD, Kim J, Sanghi P, Do D, Mancuso JJ, et al. Detection of macrophages in atherosclerotic tissue using magnetic nanoparticles and differential phase optical coherence tomography. J Biomed Opt. 2008 in press.
70. Kim J, Oh J, Kang HW, Feldman MD, Milner TE. Photothermal response of superparamagnetic iron oxide nanoparticles. Lasers Surg Med. 2008; 40:415–21. [PubMed: 18649386]
71. Oldenburg AL, Gunther JR, Boppart SA. Imaging magnetically labeled cells with magnetomotive optical coherence tomography. Opt Lett. 2005; 30(7):747–9. [PubMed: 15832926]
72. Vengrenyuk Y, Carlier S, Xanthos S, Cardoso L, Ganatos P, Virmani R, et al. A hypothesis for vulnerable plaque rupture due to stress-induced debonding around cellular microcalcifications in thin fibrous caps. Proc Natl Acad Sci USA. 2006; 103:14678–83. [PubMed: 17003118]
73. Oldenburg A, Toublan F, Suslick K, Wei A, Boppart S. Magnetomotive contrast for in vivo optical coherence tomography. Opt Express. 2005; 13:6597–614. [PubMed: 19498675]
74. Lee TM, Oldenburg AL, Sitafalwalla S, Marks DL, Luo W, Toublan FJ, et al. Engineered microsphere contrast agents for optical coherence tomography. Opt Lett. 2003; 28:1546–8. [PubMed: 12956374]
75. Yang C. Molecular contrast optical coherence tomography: A review. Photochem Photobiol. 2005; 81:215–37. [PubMed: 15588122]
76. Ma, L.; Feldman, MD.; Tam, J.; Tam, J.; Rigdon, D.; Villard, JW., et al. Small nanoclusters (nanoroses) by assembly of nanoparticle building blocks with high near infrared absorbance for cellular imaging and therapy; Abstracts of Papers, 238th ACS National Meeting; Washington, DC, United States: 2009.
77. Oh J, Feldman MD, Kim J, Kang HW, Sanghi P, Milner TE. Magneto-motive detection of tissue-based macrophages by differential phase optical coherence tomography. Lasers Surg Med. 2007; 39:266–72. [PubMed: 17295337]
78. Hirsch LR, Stafford RJ, Bankson JA, Sershen SR, Rivera B, Price RE, et al. Nanoshell-mediated near-infrared thermal therapy of tumors under magnetic resonance guidance. Proc Natl Acad Sci USA. 2003; 100:13549–54. [PubMed: 14597719]
79. Huang X, El-Sayed I, Qian W, El-Sayed M. Cancer cell imaging and photothermal therapy in the near-infrared region by using gold nanorods. J Am Chem Soc. 2006; 128:2115–20. [PubMed: 16464114]
80. O'Neal DP, Hirsch LR, Halas NJ, Payne JD, West JL. Photothermal tumor ablation in mice using near infrared-absorbing nanoparticles. Cancer Lett (Amsterdam, Netherlands). 2004; 209:171–6.

81. Jaffer FA, Weissleder R. Molecular imaging in the clinical arena. JAMA. 2005; 293:855–62. [PubMed: 15713776]
82. Weissleder R. A clearer vision for in vivo imaging. Nat Biotechnol. 2001; 19:316–7. [PubMed: 11283581]
83. Paranjape AS, Baranov S, Kuranov R, Ma L, Villard JW, Feldman MD, et al. Depth-resolved detection of nanoparticles in tissue macrophages using Phase-Sensitive Optical Coherence Tomography. 2009 In preparation.
84. Patil CA, Bosschaart N, Keller MD, van Leeuwen TG, Mahadevan-Jansen A. Combined Raman spectroscopy and optical coherence tomography device for tissue characterization. Opt Lett. 2008; 33:1135–7. [PubMed: 18483537]
85. Silveira L Jr, Sathaiah S, Zangaro RA, Pacheco MT, Chavantes MC, Pasqualucci CA. Correlation between near-infrared Raman spectroscopy and the histopathological analysis of atherosclerosis in human coronary arteries. Lasers Surg Med. 2002; 30:290–7. [PubMed: 11948599]
86. Nogueira GV, Silveira L, Martin AA, Zangaro RA, Pacheco MT, Chavantes MC, et al. Raman spectroscopy study of atherosclerosis in human carotid artery. J Biomed Opt. 2005; 10(03): 031117. [PubMed: 16229642]
87. Buschman HP, Motz JT, Deinum G, Römer TJ, Fitzmaurice M, Kramer JR, et al. Diagnosis of human coronary atherosclerosis by morphology-based Raman spectroscopy. Cardiovasc Pathol. 2001; 10:59–68. [PubMed: 11425599]
88. Romer TJ, Brennan JF 3rd, Puppels GJ, Zwinderman AH, van Duinen SG, van der Laarse A, et al. Intravascular ultrasound combined with Raman spectroscopy to localize and quantify cholesterol and calcium salts in atherosclerotic coronary arteries. Arterioscler Thromb Vasc Biol. 2000; 20:478–83. [PubMed: 10669646]
89. Caplan JD, Waxman S, Nesto RW, Muller JE. Near-infrared spectroscopy for the detection of vulnerable coronary artery plaques. J Am Coll Cardiol. 2006; 47:C92–6. [PubMed: 16631516]
90. Moreno PR, Lodder RA, Purushothaman KR, Charash WE, O'Connor WN, Muller JE. Detection of lipid pool, thin fibrous cap, and inflammatory cells in human aortic atherosclerotic plaques by near-infrared spectroscopy. Circulation. 2002; 105:923–7. [PubMed: 11864919]
91. I InfraReDx. New insight into coronary artery disease. 29 April 2009Available at: www.infraredx.com
92. Kawase Y, Suzuki Y, Ikeno F, Yoneyama R, Hoshino K, Ly HQ, et al. Comparison of nonuniform rotational distortion between mechanical IVUS and OCT using a phantom model. Ultrasound Med Biol. 2007; 33:67–73. [PubMed: 17189048]
93. Herz PR, Chen Y, Aguirre AD, Schneider K, Hsiung P, Fujimoto JG, et al. Micromotor endoscope catheter for in vivo, ultrahigh-resolutionoptical coherence tomography. Opt Lett. 2004; 29:2261–3. [PubMed: 15524374]
94. Madou, M. Fundamentals of microfabrication: The science of miniaturization. 2nd. New York, NY: CRC Press; 2002.
95. Kim KH, Park BH, Maguluri GN, Lee TW, Rogomentich FJ, Bancu MG, et al. Two-axis magnetically-driven MEMS scanning catheter for endoscopic high-speed optical coherence tomography. Opt Express. 2007; 15:18130–40. [PubMed: 19551111]
96. Yeh DT, Oralkan O, Wygant IO, O'Donnell M, Khuri-Yakub BT. 3-D ultrasound imaging using a forward-looking CMUT ring array for intravascular/intracardiac applications. Ultrasonics Ferroelec Freq Control IEEE Trans. 2006; 53:1202–11.
97. Twersky V. Absorption and multiple scattering by biological suspensions. J Opt Soc Am. 1970; 60:1084. [PubMed: 5480400]
98. Steinke JM, Shepherd AP. Role of light-scattering in whole-blood oximetry. IEEE Trans Biomed Eng. 1986; 33:294–301. [PubMed: 3957382]
99. Roggan A, Friebel M, Dorschel K, Hahn A, Muller G. Optical properties of circulating human blood in the wavelength range 400-2500 NM. J Biomed Opt. 1999; 4:36–46. [PubMed: 23015168]
100. Villard JW, Feldman MD, Kim J, Milner TE, Freeman GL. Use of a blood substitute to determine instantaneous murine right ventricular thickening with optical coherence tomography. Circulation. 2002; 105:1843–9. [PubMed: 11956129]

101. de Boer JF, Cense B, Park BH, Pierce MC, Tearney GJ, Bouma BE. Improved signal-to-noise ratio in spectral-domain compared with time-domain optical coherence tomography. Opt Lett. 2003; 28:2067–9. [PubMed: 14587817]
102. Yun S, Tearney G, de Boer J, Iftimia N, Bouma B. High-speed optical frequency-domain imaging. Opt Express. 2003; 11:2953–63. [PubMed: 19471415]
103. Yun SH, Boudoux C, Pierce MC, Boer JFD, Tearney GJ, Bouma BE. Extended-cavity semiconductor wavelength-swept laser for biomedical imaging. Photon Technol Lett IEEE. 2004; 16:293–5.
104. Yun SH, Boudoux C, Tearney GJ, Bouma BE. High-speed wavelength-swept semiconductor laser with a polygon-scanner-based wavelength filter. Opt Lett. 2003; 28:1981–3. [PubMed: 14587796]
105. Huber R, Wojtkowski M, Fujimoto JG. Fourier Domain Mode Locking (FDML): A new laser operating regime and applications for optical coherence tomography. Opt Express. 2006; 14:3225–37. [PubMed: 19516464]
106. Huber R, Adler DC, Fujimoto JG. Buffered Fourier domain mode locking: Unidirectional swept laser sources for optical coherence tomography imaging at 370,000 lines/s. Opt Lett. 2006; 31:2975–7. [PubMed: 17001371]
107. Nadkarni SK, Pierce MC, Park BH, de Boer JF, Whittaker P, Bouma BE, et al. Measurement of collagen and smooth muscle cell content in atherosclerotic plaques using polarization-sensitive optical coherence tomography. J Am Coll Cardiol. 2007; 49:1474–81. [PubMed: 17397678]
108. Bauriedel G, Hutter R, Welsch U, Bach R, Sievert H, Luderitz B. Role of smooth muscle cell death in advanced coronary primary lesions: Implications for plaque instability. Cardiovasc Res. 1999; 41:480–8. [PubMed: 10341848]
109. Newby AC, Zaltsman AB. Fibrous cap formation or destruction—the critical importance of vascular smooth muscle cell proliferation, migration and matrix formation. Cardiovasc Res. 1999; 41:345–60. [PubMed: 10341834]
110. Rekhter MD, Hicks GW, Brammer DW, Hallak H, Kindt E, Chen J, et al. Hypercholesterolemia causes mechanical weakening of rabbit atheroma: Local collagen loss as a prerequisite of plaque rupture. Circ Res. 2000; 86:101–8. [PubMed: 10625311]
111. Nadkarni SK, Bouma BE, Yelin D, Gulati A, Tearney GJ. Laser speckle imaging of atherosclerotic plaques through optical fiber bundles. J Biomed Opt. 2008; 13:054016. [PubMed: 19021396]
112. Oh WY, Yun SH, Vakoc BJ, Shishkov M, Desjardins AE, Park BH, et al. High-speed polarization sensitive optical frequency domain imaging with frequency multiplexing. Opt Express. 2008; 16:1096–103. [PubMed: 18542183]
113. Bovik, AC. The handbook of image and video processing. 2nd. New York, NY: Academic Press; 2005.
114. Iftimia N, Bouma BE, Tearney GJ. Speckle reduction in optical coherence tomography by “path length encoded” angular compounding. J Biomed Opt. 2003; 8:260–3. [PubMed: 12683852]
115. Pircher M, Gotzinger E, Leitgeb R, Fercher AF, Hitzenberger CK. Speckle reduction in optical coherence tomography by frequency compounding. J Biomed Opt. 2003; 8:565–9. [PubMed: 12880365]
116. Ozcan A, Bilenca A, Desjardins AE, Bouma BE, Tearney GJ. Speckle reduction in optical coherence tomography images using digital filtering. J Opt Soc Am A. 2007; 24:1901–10.
117. Adler DC, Ko TH, Fujimoto JG. Speckle reduction in optical coherence tomography images by use of a spatially adaptive wavelet filter. Opt Lett. 2004; 29:2878–80. [PubMed: 15645810]
118. Tearney GJ, Bouma BE. Atherosclerotic plaque characterization by spatial and temporal speckle pattern analysis. Opt Lett. 2002; 27:533–5. [PubMed: 18007856]
119. Huang C, Liu B, Brezinski ME. Ultrasound-enhanced optical coherence tomography: Improved penetration and resolution. J Opt Soc Am A. 2008; 25:938–46.

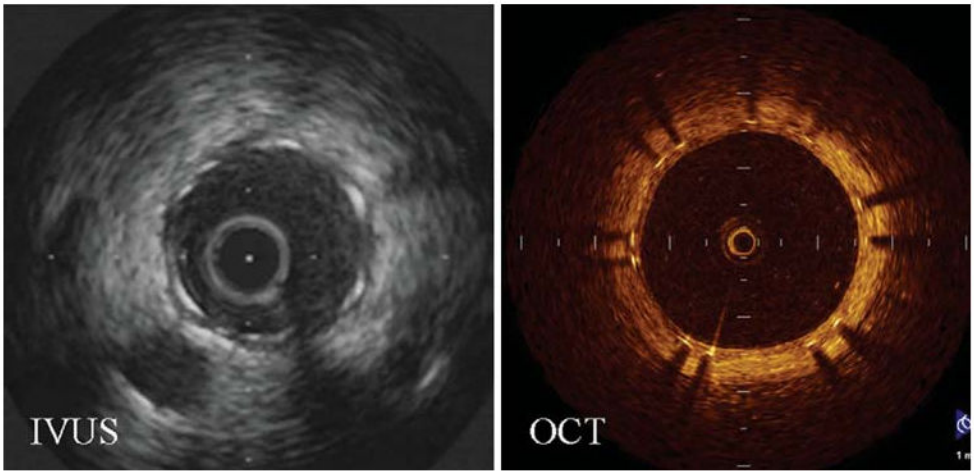

Figure 1.

Representative cross-sectional images that demonstrate the superiority of OCT over IVUS in resolving neointima growth at the clinically important 6-month follow-up. Images were obtained at the same distance from a major side branch (Reproduced with permission from[14]).

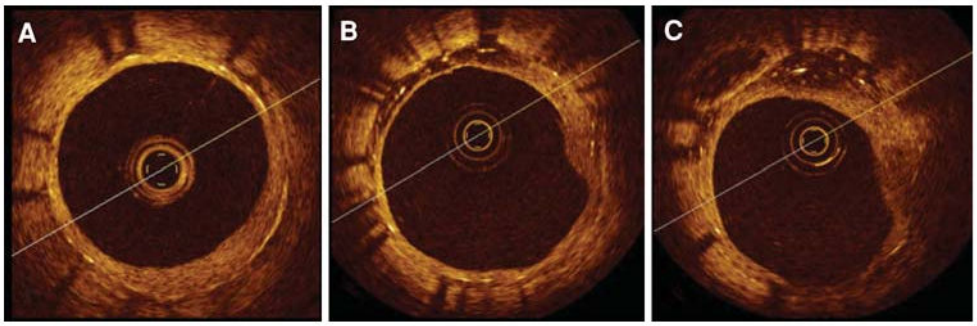

Figure 2.

Heterogeneous vessel response in a paclitaxel-eluting stent recorded at 13 months during elective OCT follow up. Significant differences in vessel response were observed in this short segment along the same stent. (**A**) stent coverage of neointima; (**B-C**) asymmetrical neointimal coverage with signal attenuation (“black holes”) of the tissue growth from 9 o'clock to 12 o'clock (Reproduced with permission from[36]).

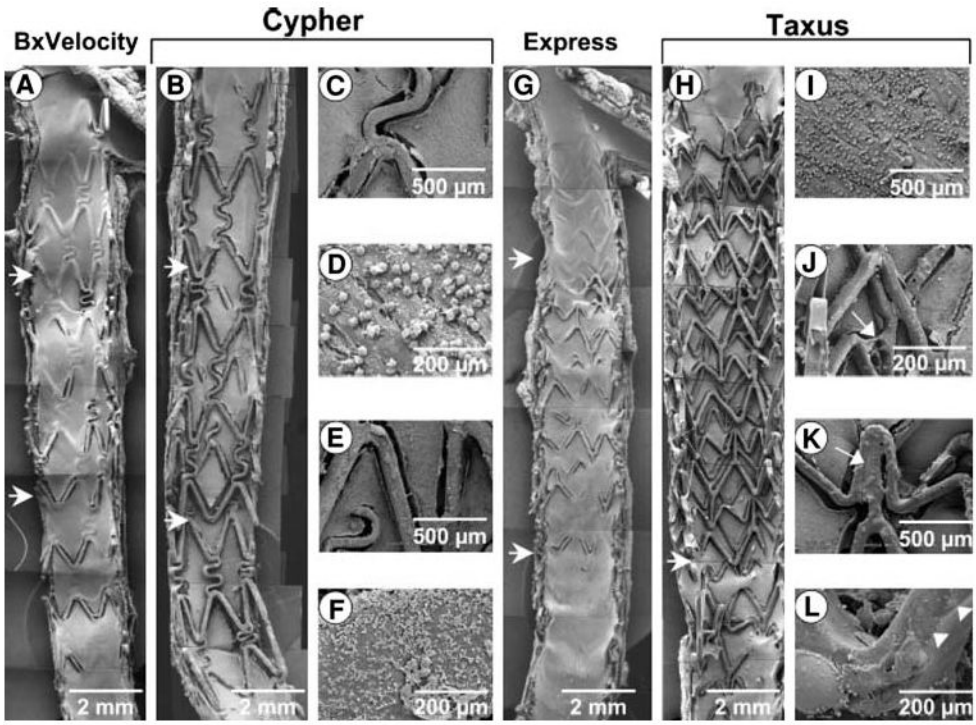

Figure 3.

SEM of overlapping 28-day BxVelocity (**A**), Cypher (**B-F**), Express (**G**), and Taxus (**H-L**) stents. Regions of overlap are within horizontal arrows. There is less surface coverage by endothelial cells on Taxus than Cypher stents, specifically in segments of overlap. Overlapping segments within BxVelocity and Express stents showed far greater endothelialization than DES. Higherpower views of Cypher stents (**C-F**) from segment of overlap show adherent platelets and inflammatory cells on stent struts and adjoining neointima. Higherpower images from overlapping segments of Taxus stents (**I-L**) show greater inflammatory infiltrate (**I**), polymer sticking and stretching across stent struts (**J**, *arrow*), unexpanded struts (**K**, *arrow*), and irregular distribution of the polymer over stent strut surface (**L**, *arrowheads*) (Reproduced with permission from[39]).

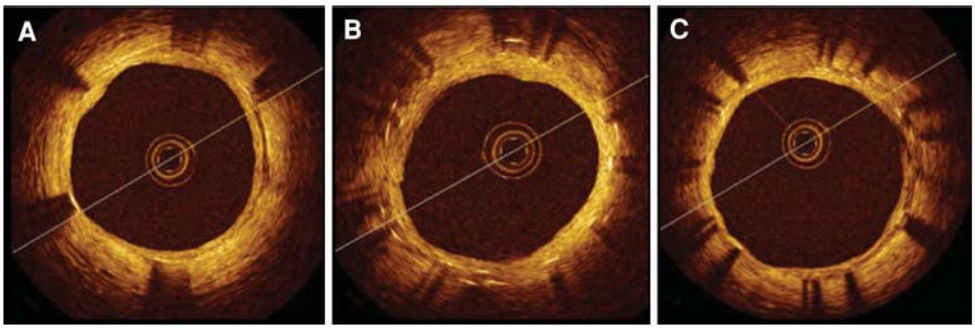

Figure 4.

OCT cross-sectional images of multiple CypherTM stents in overlap implanted in a long lesion. Elective follow-up at 6 months after the implant. (**A**) distal stent; (**B**) overlapping segment with dual strut layers; (**C**) proximal stent. Well-apposed stent struts at all cross sections with uniform coverage and minimal neointimal growth. No differences were observed between single and double layer responses[36].

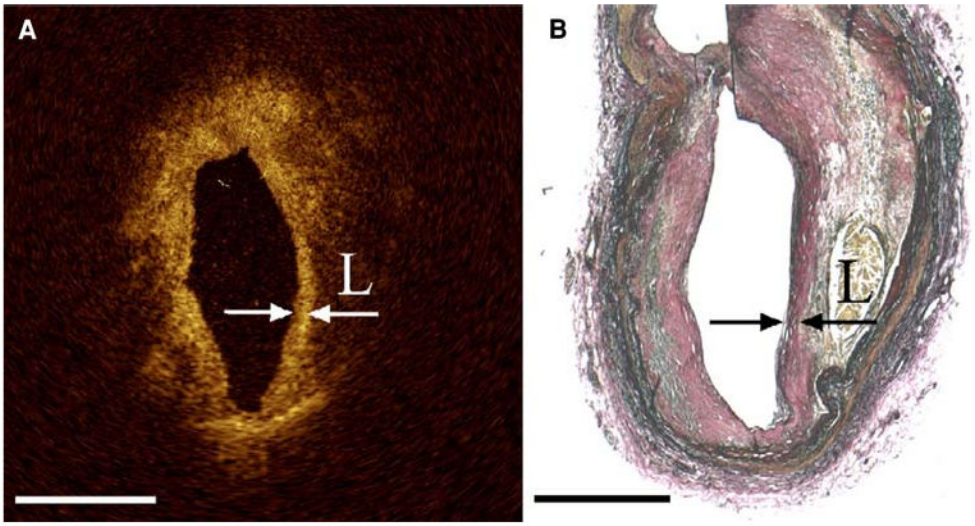

Figure 5.

(**A**) OCT image with *arrows* indicating the borders of a thin fibrous cap overlying a lipid pool with corresponding histology (**B**) Note that the "back wall" of the lipid core is poorly visualized with OCT due to light attenuation (Reproduced with permission from[47]).

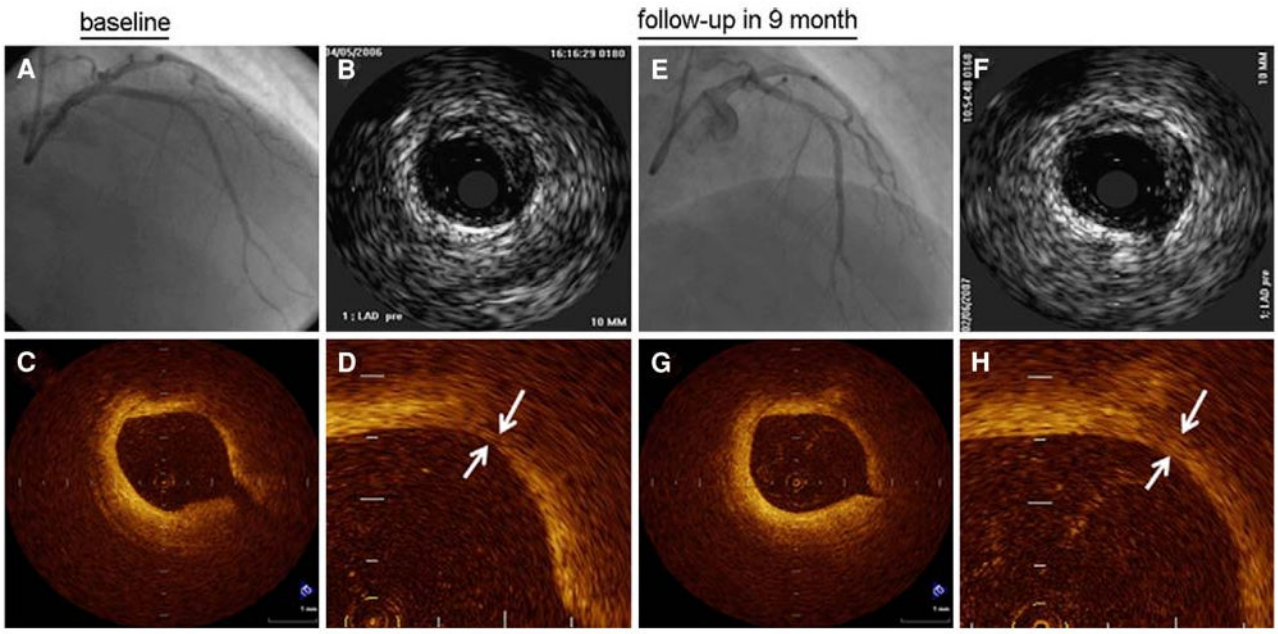

Figure 6.

Angiography (**A, E**) and IVUS (**B, F**) images from a patient before and after statin therapy with corresponding OCT images in the bottom row. Before statin therapy, the patient's fibrous cap thickness (indicated by *white arrows* in **D**) was 110 μm and increased to 320 μm (*white arrows* in **H**) at 9-month follow-up[49].

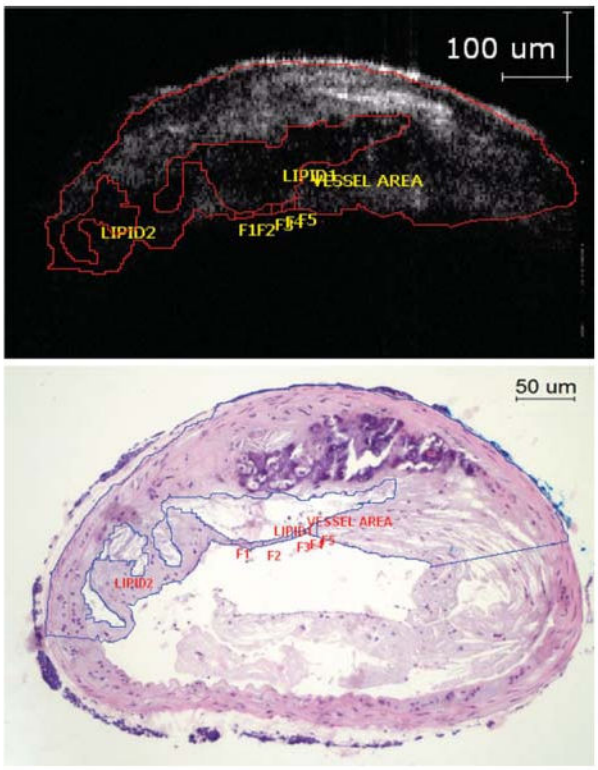

Figure 7.

The OCT image (*above*) shows areas with poor signal corresponding to lipid rich areas as seen from the histology (*below*). The lipid core size can be accurately measured and expressed as a percentage of the total plaque (21.4% via OCT compared to 19.7% via histology for this study). Note the inability of OCT to visualize the lower arterial wall due to light attenuation (Reproduced with permission from[53]).

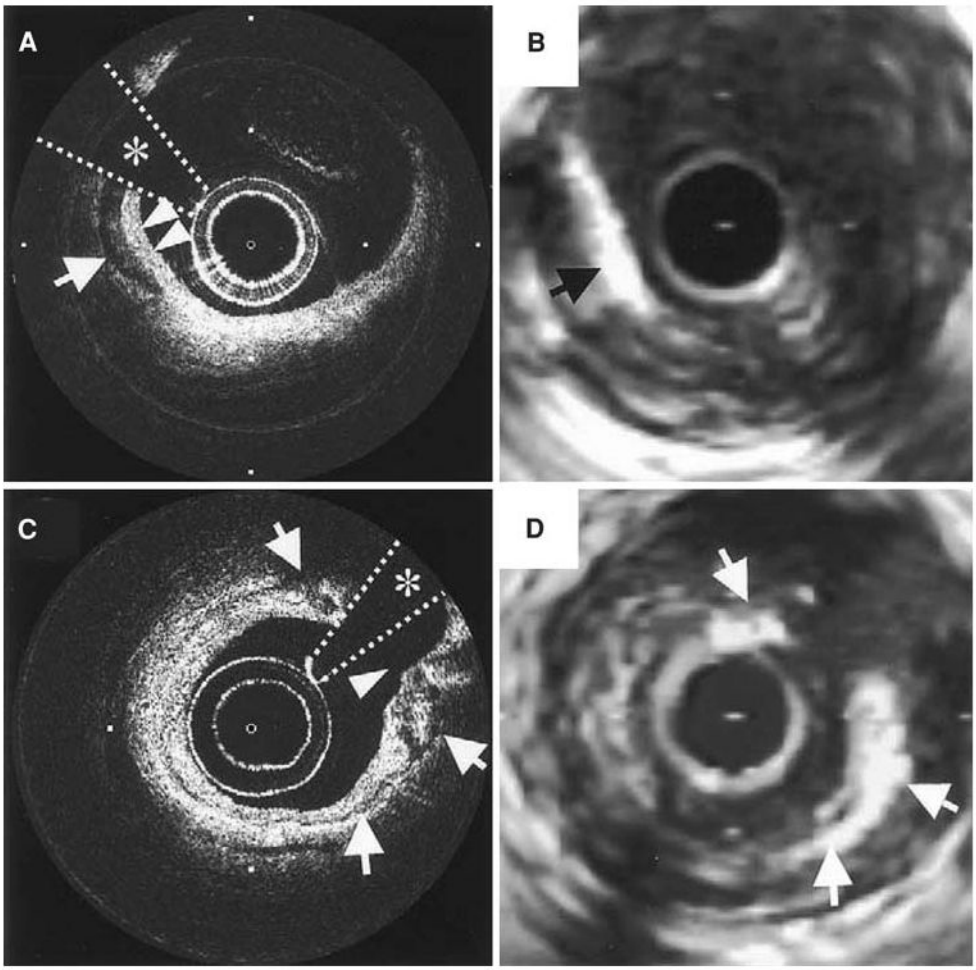

Figure 8.

(**A, C**) OCT images of a coronary plaque with corresponding IVUS (**B, D**) images. The *arrow* in **A** points to a well-delineated and signal-poor area corresponding to a macro-calcification which is also seen in the IVUS image (**B**). Notice that in **A** the borders of the overlying fibrous tissue and calcification are “in focus” whereas in the IVUS image, the bright echo from the calcification obscures the features of the fibrous tissue. In image **C**, the *arrows* denote a thin layer of circumferential calcification with the surrounding features well defined unlike in the corresponding IVUS image (**D**)[54].

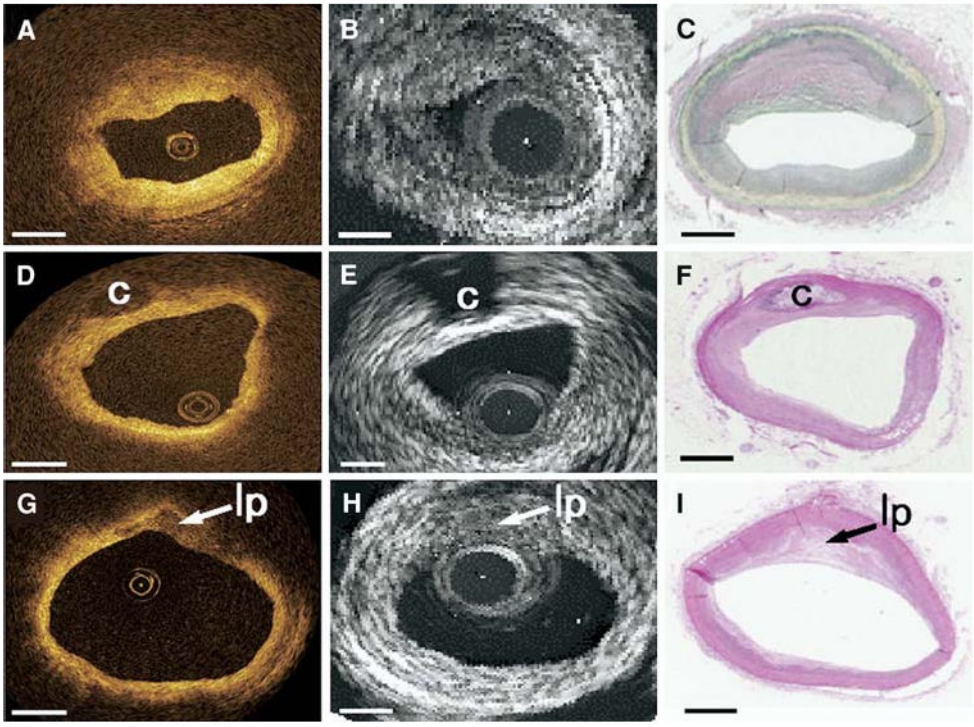

Figure 9.

Comparison of the three types of plaque (fibrous, fibrocalcific, and lipid-rich) as identified with OCT, IVUS, and histology. The top row shows homogeneous, signal-rich regions that characterize the fibrous plaque in OCT, which is difficult to differentiate with gray scale IVUS. The middle row shows a fibrocalcific plaque which appears as well-delineated signal-poor regions with sharp borders for OCT and bright echolucent regions in IVUS. Lipid-rich plaques are on the bottom row, which appear as signal-poor regions with diffuse borders on OCT and IVUS (Reproduced with permission from[58]).

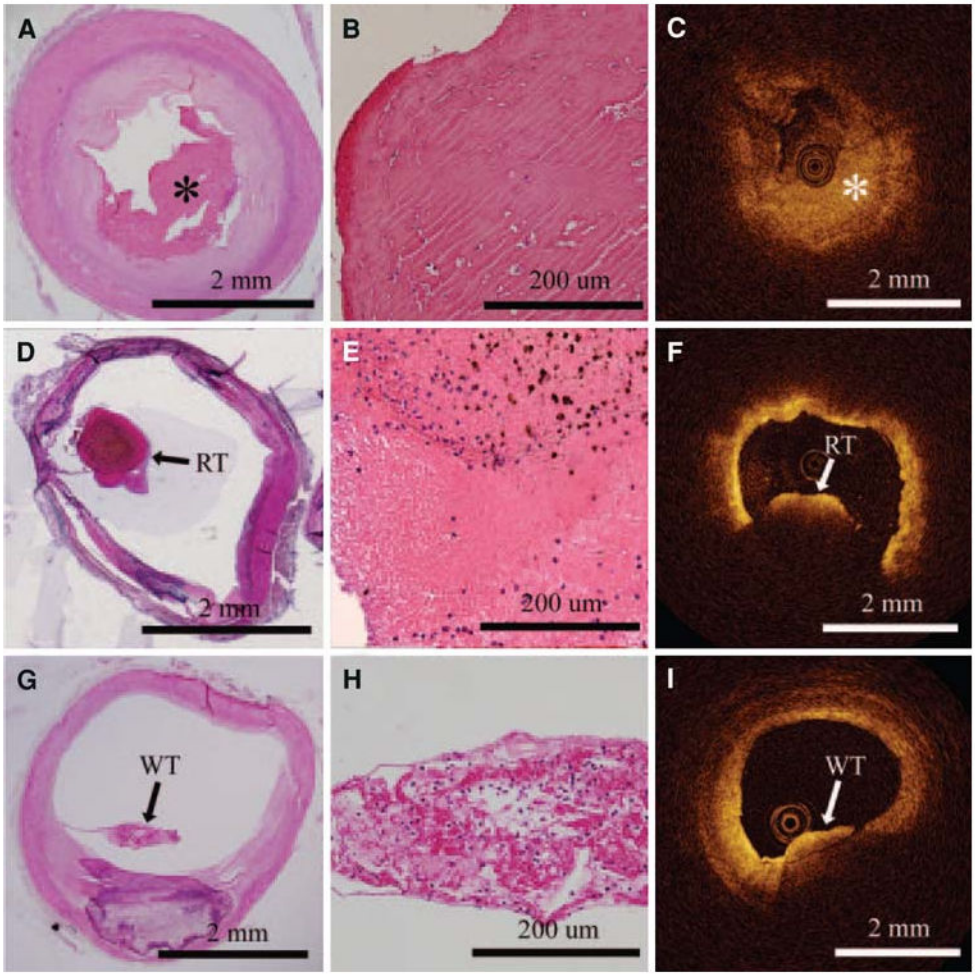

Figure 10.

OCT images on the right are correlated with histology images on the left. The top row shows a fibrous clot (*asterisk*), comprising fibrin and a few red blood cells. The middle row shows a red thrombus by histology, which is evident in the OCT image by the large shadow from the thrombus (light attenuation) that prevents visualization of the entire arterial wall. White thrombus, composed predominantly of platelets, is in the last row. White thrombus can be discriminated from the red thrombus in the OCT image since the entire thickness of the clot and arterial lumen can be seen behind the thrombus[59].

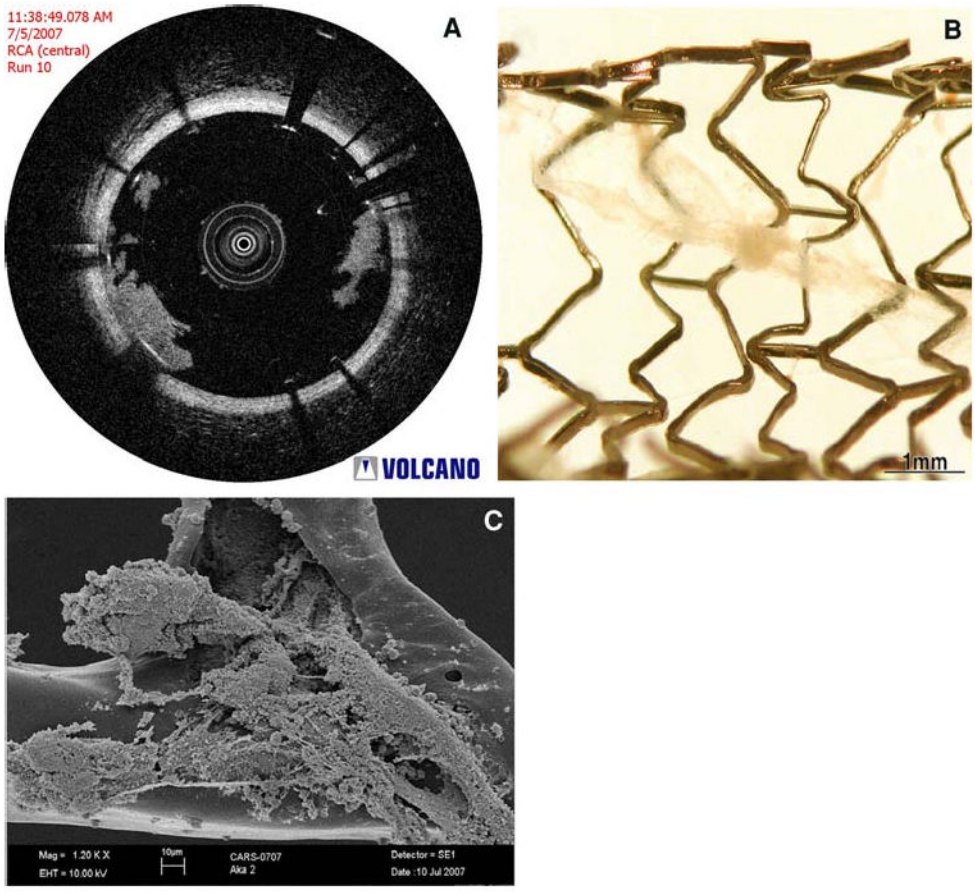

Figure 11.

(**A**) OCT image from an in vivo porcine coronary artery which demonstrates the presence of a white thrombus on a bare metal stent, which was extracted from the coronary artery (**B**) (courtesy of Volcano Corporation, San Antonio, TX and Rancho Cordova, CA). This material was then imaged with electron microscopy (**C**), which verified that the structure contains platelets and cellular debris, corresponding to white thrombus (Images courtesy of Dr. Fermin Tio, Texas Veterans Affairs Health System, San Antonio, TX).

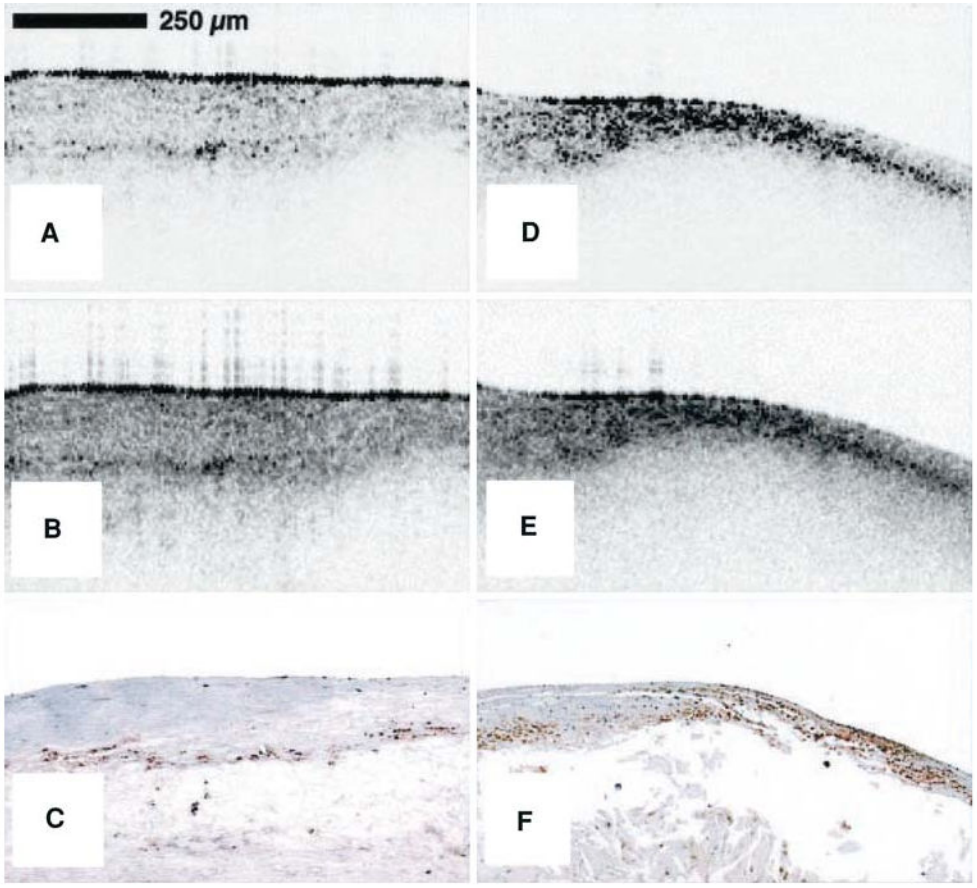

Figure 12.

Raw (**A**) and logarithm base 10 (**B**) OCT images of a post-mortem fibroatheroma with a low density of macrophages within the fibrous cap. (**C**) Corresponding histology for **A** and **B** (CD68 immunoperoxidase; original magnification ×100). Raw (**D**) and logarithm base 10 (**E**) OCT images of a fibroatheroma with a high density of macrophages within the fibrous cap. (**F**) Corresponding histology for **D** and **E** (CD68 immunoperoxidase; original magnification (×100)[67].

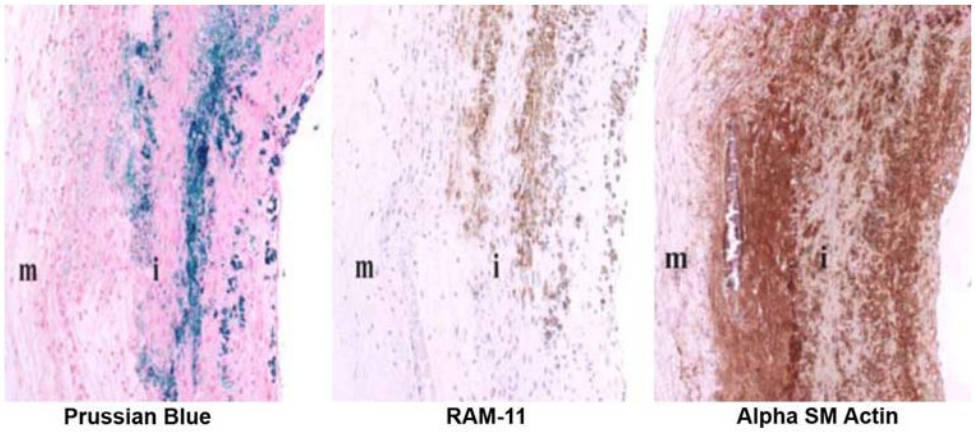

Figure 13.

Histologic images of double-balloon injured fat-fed abdominal aorta from a New Zealand white rabbit demonstrating co-localization of macrophages and iron nanoparticles. *Left*: section stained with Prussian blue for iron; *Middle*: section stained with RAM-11 for macrophages; *Right*: section stained for SM actin for SM cells; i = intima; m = media (Reproduced with permission from[69]).

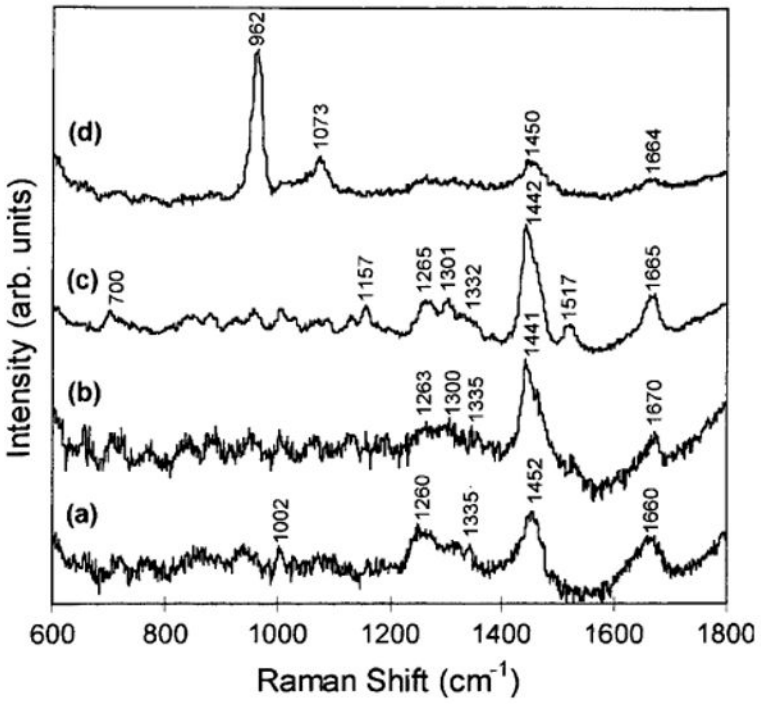

Figure 14.

In vitro near-infrared Raman spectra obtained from human coronary artery tissues: (a) non-atherosclerotic, (b) atherosclerotic composed mainly of macrophage foam cells and lipid-laden smooth muscle cells, (c) atherosclerotic covered by a fibrous connective tissue, and (d) calcified (Reproduced with permission from[85]).

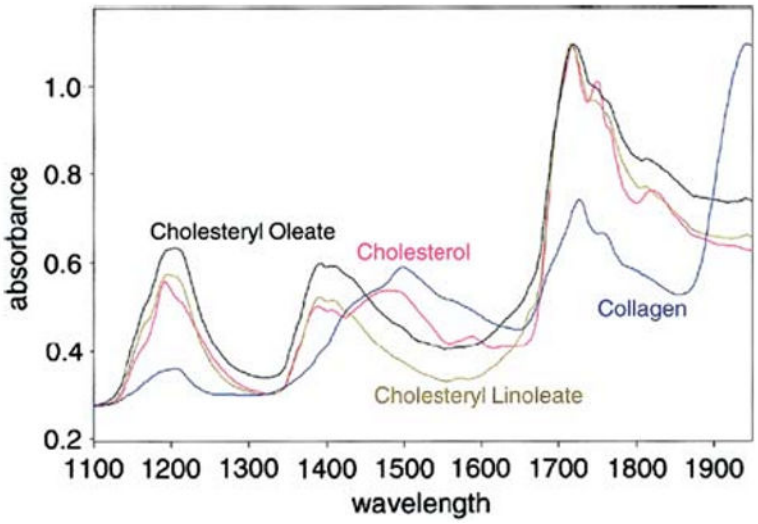

Figure 15.

NIR spectra of various pure substances possibly related to plaque vulnerability (Reproduced with permission from[89]).

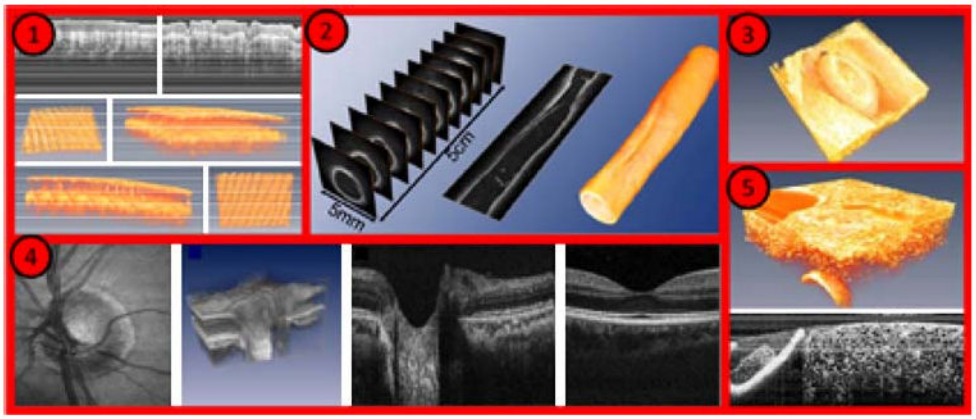

Figure 16.

Imaging examples with Fourier Domain-Mode Locked lasers: (1) human skin in vivo, (2) endoscopic intravascular 3D data set of a 5-cm segment of an excised radial artery from a cadaver, (3) heart of a quail embryo, (4) human retina in vivo, (5) high resolution OCT of a cucumber (adapted from http://spie.org/x33321.xml?ArticleID=x33321).

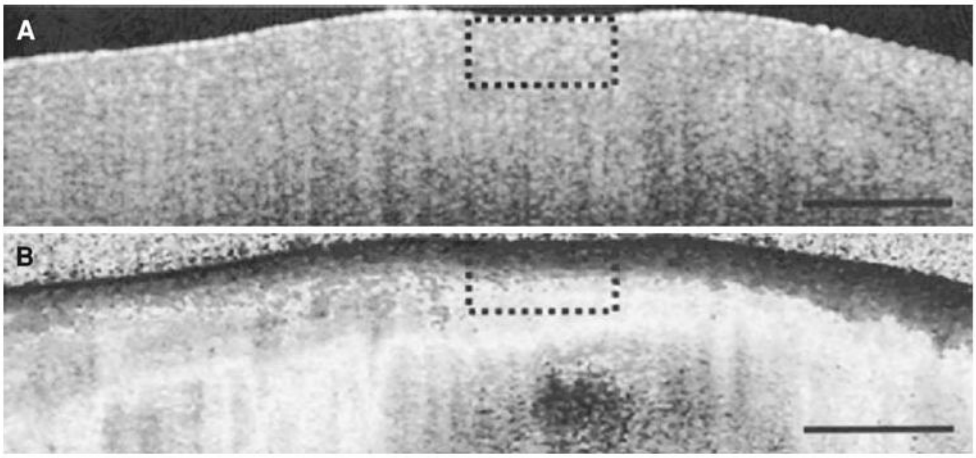

Figure 17.

(**A**) Optical coherence tomography images of a fibrous cap, demonstrating difficulty in identifying fibrous cap thickness. (**B**) The addition of Polarization-sensitive optical coherence tomography (PS-OCT) provides additional contrast between the fibrous cap and the remainder of the plaque allowing a more precise measurement of the fibrous cap thickness (Reproduced with permission from[107]).